

Article

Dynamic Assessment of the Flood Risk at Basin Scale under Simulation of Land-Use Scenarios and Spatialization Technology of Factor

Jun Liu ¹, Jiyan Wang ¹, Junnan Xiong ^{1,2,*}, Weiming Cheng ², Xingjie Cui ¹, Wen He ¹, Yufeng He ¹, Yu Duan ¹, Gang Yang ¹ and Nan Wang ³

- ¹ School of Civil Engineering and Geomatics, Southwest Petroleum University, Chengdu 610500, China; 201922000655@stu.swpu.edu.cn (J.L.); wangjiyan@swpu.edu.cn (J.W.); 202022000943@stu.swpu.edu.cn (X.C.); 201922000663@stu.swpu.edu.cn (W.H.); 201922000656@stu.swpu.edu.cn (Y.H.); 201922000658@stu.swpu.edu.cn (Y.D.); 201922000664@stu.swpu.edu.cn (G.Y.)
- ² State Key Laboratory of Resources and Environmental Information System, Institute of Geographic Sciences and Natural Resources Research, CAS, Beijing 100101, China; chengwm@reis.ac.cn
- ³ School of Geographical Sciences, Northeast Normal University, Changchun 130024, China; wangn236@nenu.edu.cn
- * Correspondence: xiongjn@swpu.edu.cn



Citation: Liu, J.; Wang, J.; Xiong, J.; Cheng, W.; Cui, X.; He, W.; He, Y.; Duan, Y.; Yang, G.; Wang, N. Dynamic Assessment of the Flood Risk at Basin Scale under Simulation of Land-Use Scenarios and Spatialization Technology of Factor. *Water* **2021**, *13*, 3239. <https://doi.org/10.3390/w13223239>

Academic Editors: Fazlul Karim, Zaved Khan and Tawatchai Tingsanchali

Received: 10 October 2021
Accepted: 8 November 2021
Published: 15 November 2021

Publisher's Note: MDPI stays neutral with regard to jurisdictional claims in published maps and institutional affiliations.



Copyright: © 2021 by the authors. Licensee MDPI, Basel, Switzerland. This article is an open access article distributed under the terms and conditions of the Creative Commons Attribution (CC BY) license (<https://creativecommons.org/licenses/by/4.0/>).

Abstract: Climate change, population increase, and urban expansion have increased the risk of flooding. Therefore, accurately identifying future changing patterns in the flood risk is essential. For this purpose, this study elaborated a new framework for a basin scale that employs a future land-use simulation model, a factor spatialization technique, and a novel hybrid model for scenario-based flood risk assessment in 2030 and 2050. Three land-use scenarios (i.e., natural growth scenario, cropland protection scenario, and ecological protection scenario) were set and applied in Jinjiang Basin to explore the changes in future flood risk under these scenarios. The results indicate the different degrees of increase in flood risk that will occur in the three scenarios. Under the natural growth (NG) scenario, the city will expand rapidly with the growth of population and economy, and the total area with high and very high flood risk will increase by 371.30 km² by 2050, as compared to 2020. However, under the ecological protection (EP) scenario, woodlands will be protected, and the growth in population, economy, and built-up lands will slow down with slightly increased risk of flooding. In this scenario, the total area with high and very high flood risk will increase by 113.75 km² by 2050. Under the cropland protection (CP) scenario, the loss of croplands will have been effectively stopped, and the flood risk will not show a significant increase under this scenario, with an increase by only 90.96 km² by 2050, similar to the EP scenario. Spatially, these increased flood risks mainly locate at the periphery of existing built-up lands, and the high-flood-risk zones are mainly distributed in the southeast of the Jinjiang Basin. The information about increasing flood risk determined by the framework provides insight into the spatio-temporal characteristics of future flood-prone areas, which facilitates reasonable flood mitigation measures to be developed at the most critical locations in the region.

Keywords: dynamic flood risk assessment; future land-use simulation; scenario-based planning; spatialization technology; Markov chains; ANN; FLUS model; TOPSIS

1. Introduction

Flood is considered to be the natural disaster responsible for the most severe losses of economy and lives [1], with economic losses caused by flood constituting 31% of the total losses resulting from natural disasters globally [2]. According to the report, flood leads to about 20,000 deaths and 75 million affected people each year in the whole world [3]. In 2010, for example, approximately 178 million people were affected by flooding, and the total losses recorded during 1998 and 2010 exceeded USD 40 billion worldwide [4]. In

China, floods are particularly serious, due to the effect of East Asian monsoon [5]. Since 1990, China has suffered an average annual economic loss of about \$17 billion caused by flooding, with two-thirds of its territory and more than half of its total population affected by floods [1]. Therefore, considering the severity of consequential damage caused by floods, it is necessary to implement flood control and prevention measures. However, before taking targeted measures to control floods, the likelihood of flooding, potential losses, and resilience must be assessed first [6]. In this regard, flood risk assessment as a nonstructural measure has been widely taken into account to identify the areas more susceptible to floods [7].

The ongoing climate change and socioeconomic development have direct impacts on floods [8], which will lead to the rise of the frequency and magnitude of future flood situations [7]. In addition, due to the population increase and the rapid growth of urban expansion, the risk level and spatial distribution of floods will change over time [9,10]. Thus, the flood risk is considered to be dynamic, which can be attributed to land-use change, population expansion, and property accumulation [6]. Although the directions of future land-use change are diverse, most previous studies have assessed the flood risk statically based on one-period data, and few studies have taken the future land-use scenarios into account when assessing flood risk [11]. In this regard, Lai et al. have assessed the future flood risk in Dongjiang Basin based on two land-use maps drawn for 2030 and 2050 [6]. Liu et al. have drawn four land-use maps under a planning scenario in the years of 1954, 1982, 2000, and 2020, to analyze the impact of land-use changes on flood exposure of Wuhan [12]. However, the different future land-use change scenarios were ignored in their study. In this case, how to consider different land-use change scenarios in the dynamic assessment of flood risk is an urgent issue to be addressed. In this context, future land-use simulation (FLUS) model and Markov model were applied to simulate the land-use changes under three scenarios in this study. The Markov model is able to predict the amounts of future land-use types under different scenarios. The FLUS model can efficiently integrate the relationship between land-use changes and driving factors by embedding with an ANN, and thus can generate more realistic simulations [13]. These two models can be used together for the simulation of future land-use changes in different scenarios, and then these can be taken into account in the the flood risk assessment.

In the future scenarios, forecasting population size and economic conditions is essential for assessing the hazard-bearing bodies. However, most of the existing studies used only one aggregate value, i.e., a region with only one value, as the predicting value of future population (POP) and Gross Domestic Product (GDP) [14,15]. The interior spatial distributions of the POP and GDP have not been focused on, leading to the low spatial accuracy in the assessment. In this regard, some efforts have been made by Lai et al. [6], who distributed the increased POP and GDP over urban land and obtained the spatial distribution of them over urban land. However, their study only takes into account the impact of building-up lands, without extensively considering changes in other land-use types. In this case, a spatialization technique was introduced into the flood risk assessment to obtain a fine spatial distribution of factors instead of a lumped/overall value.

For the flood risk determination, various models have been developed, and these can be broadly classified into three categories, namely, physically based simulation models, sampling models, and nonsampling models [6]. As effective flood inundation models, the physically based simulation models can provide the details of floods according to the 1D or 2D hydraulic models, such as inundation extent, the water depth, and the velocity [16]. However, since a sea of input data and substantial computational resources are required in these models, the application of them for regional-scale analysis is limited [17]. The sampling models and nonsampling models do not take into account the complex hydrologic or hydrodynamic processes, and they describe a relationship between flood risk levels and flood factors [18]. Therefore, they are widely used in regional-scale flood analysis. At present, as sampling models, the machine learning models (i.e., support vector machine [19], random forest [20], artificial neural network [21], and decision tree [22]) and

statistical models (i.e., weights-of-evidence [23], frequency ratio [22], and evidence belief function [24]) are popular for the flood risk assessment. However, the samples based on historical flooding locations become essential for the implementation of these sampling models, which results in their unattractive applications for data-poor regions. Compared to the sampling models, nonsampling models can assess the flood risk without the samples but based on the knowledge of experts or data information. However, the nonsampling models are considered to be subjective; among them, analytic hierarchy process (AHP) is the most typical [25,26]. Although the uncertainty of the AHP cannot be eliminated, it can be mitigated by applying fuzzy numbers in the traditional AHP [27]. Therefore, the triangular fuzzy number-based AHP (TFN-AHP) was selected as a subjective method to determine the flood risk in this study. Further, considering that combining objective and subjective results allows for a more reasonable assessment of the object [28], an objective nonsampling method was also taken into account in this study. Generally, objective nonsampling models are conducted based on data information, including criteria importance through intercriteria correlation (CRITIC) [29], technique for order preference by similarity to an ideal solution (TOPSIS) [30], entropy weighting method [31], and coefficient of variation method [32]. Among them, the advantage of TOPSIS is obvious, as explicit trade-offs and interactions among attributes are allowed [33]. However, the single TOPSIS method focuses only on the final scores of different evaluation objects and ignores the heterogeneity among the attributes of these objects, which can be quantified by methods such as CRITIC [34]. Therefore, a hybrid model (CRITIC-TOPSIS) was proposed by integrating the CRITIC and TOPSIS models. Although the CRITIC has shown good performance in determining weights [35], it is rarely employed for the evaluation of inhomogeneities and the generation of decision support options. Therefore, the CRITIC warrants consideration. To the best of our knowledge, this is the first time that CRITIC and TOPSIS have been combined, which enriches the means of flood risk determination.

In this context, the main purpose of this study is to propose a new framework to assess future flood risk dynamically, which provides a practical way to explore the complex relationship between changes in future flood risk and the state of social development. In this framework, land-use types under three scenarios in 2030 and 2050 were simulated by Markov chain model and FLUS model. Then, the factor spatialization technique was introduced to determine spatial distribution of hazard-bearing bodies (i.e., POP and general budget revenue (GBR)). Notably, due to the availability of data, the GBR was used instead of GDP to reflect the economic level of the region. Finally, each future flood risk map under the three scenarios was obtained by combining a subjective risk map generated by TFN-AHP and an objective risk map generated by the novel hybrid model of CRITIC and TOPSIS (CRITIC-TOPSIS). By applying this framework in Jinjiang Basin, changes in flood risk under three land-use scenarios from 2020 to 2050 are revealed in this study. These findings not only facilitate a more comprehensive insight into the challenges posed by future social development on flood risk, but also provide scientific and practical merit for the future flood mitigation measures.

2. Materials

2.1. Study Area

This study is focused on the Jinjiang Basin (24°31′–33°39′ N, 117°44′–118°47′ E), which is located in the southeast coast of Fujian Province, China (Figure 1). The whole Jinjiang Basin is within the Quanzhou City, a coastal city in the Western Taiwan Straits Economic Zone of China [36]. Therefore, the economy of the study area is developed, with the GDP exceeding one trillion yuan in 2020. However, as the economy continues to develop, so does the exposure, which increases the risk of flooding. There are two tributaries flowing through this basin, the Dongxi and Xixi rivers. The area of Jinjiang Basin is about 5294 km² at an altitude varying from 1 to 1516 m. The terrain in the study area is complex, including the low plain in the southeast and the mountainous area in the northwest part of the basin. In terms of climate, the Jinjiang Basin area is characterized by a subtropical

monsoon climate and has an average annual temperature and precipitation level of 20 °C and 1686 mm, respectively [37]. Notably, about 80% of the annual total precipitations are concentrated in the period of April to September, which leads to flooding easily [36,37].

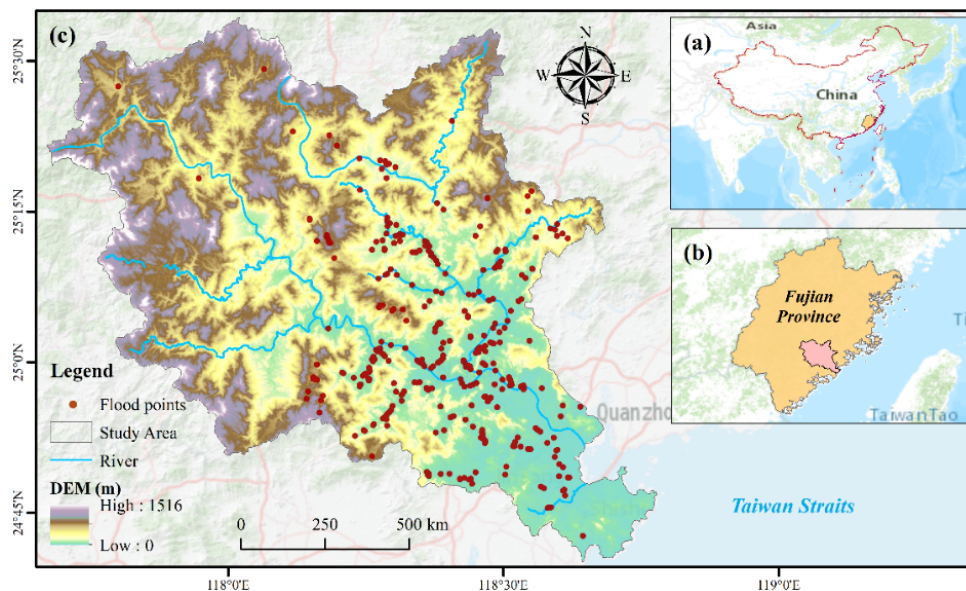


Figure 1. The study area of Jinjiang Basin: (a) Fujian province in China; (b) Jinjiang Basin in Fujian province; (c) digital elevation model (DEM), and location of the main river in Jinjiang Basin.

During the last few decades, the Jinjiang Basin has been highly affected by flooding. According to the statistics provided by the National Flash Flood Investigation and Evaluation Project, 359 floods occurred in the Jinjiang Basin during 1949–2018, and have led to huge loss of life and property. Taking 2010 as an example, a total of 14 flash floods caused 2 deaths and 95.6 million yuan of economic losses. Under these circumstances, it is meaningful to perform flood risk assessment for this basin.

2.2. Data

In the flood risk assessment, the first task is to construct a spatial database that contains the flood factors. However, the suitable flood factors vary with the characteristics of the different areas [22], and the same factors have very different influences in different areas [21]. In this study, considering the characteristics of Jinjiang Basin and referring to the existing studies [6], three aspects of data were selected (i.e., disaster-inducing factors, disaster-breeding environments, and hazard-bearing bodies). The primary sources of the factors are presented in Table 1, and each of them was converted into a gridded database with a spatial resolution of 100 m × 100 m in ArcGIS. In addition, the data used in the future land-use simulation are shown in the Table S1 (Supporting Information).

Table 1. Primary sources for the factors used for flood assessment in this study.

Data Aspect	Sub-Factors	Data	Time	Source of Data	Resolution
Disaster-inducing factors	M3DP	GPM	2000–2020	National Aeronautics and Space Administration (https://disc.gsfc.nasa.gov/datasets/GPM_3IMERGDE_06/summary?keywords=GPM) (accessed on 18 April 2021)	0.1° × 0.1°
	R50 mm				
Disaster-breeding environments	DEM	DEM	2010	Geospatial Data Cloud (www.gscloud.cn) (accessed on 6 May 2021)	30 m × 30 m
	Slope				
	TWI				

Table 1. Cont.

Data Aspect	Sub-Factors	Data	Time	Source of Data	Resolution
	DR	River	2013	National Flash Flood Investigation and Evaluation Project (NFFIEP)	1:1,000,000
	RC	Land-use	2020	Globeland30 (http://www.globeland30.com/) (accessed on 20 May 2021)	30 m × 30 m
Hazard-bearing bodies	POP	Quanzhou statistical yearbook	2020	Quanzhou Statistical Information network (http://tjj.quanzhou.gov.cn/tjzl/tjsj/nds/) (accessed on 1 June 2021)	\
	GBR	Quanzhou statistical yearbook			

The disaster-inducing factors contained the maximum three-day precipitation (M3DP) and number of days with daily rainfall ≥ 50 mm (R50 mm), which reflect the intensity and frequency of precipitation, respectively. The M3DP (Figure 2a) has been proven to have a strong correlation with the flooding [38] and has been successfully applied in the analysis of flood susceptibility and risk [25,39]. Similarly, the R50 mm (Figure 2b) is strongly associated with flooding, due to the fact that frequent heavy precipitation tends to lead to flooding. These two factors were obtained by Kriging interpolation method, according to the annual mean M3DP (2000–2020) calculated by GPM data (Global Precipitation Measurement).

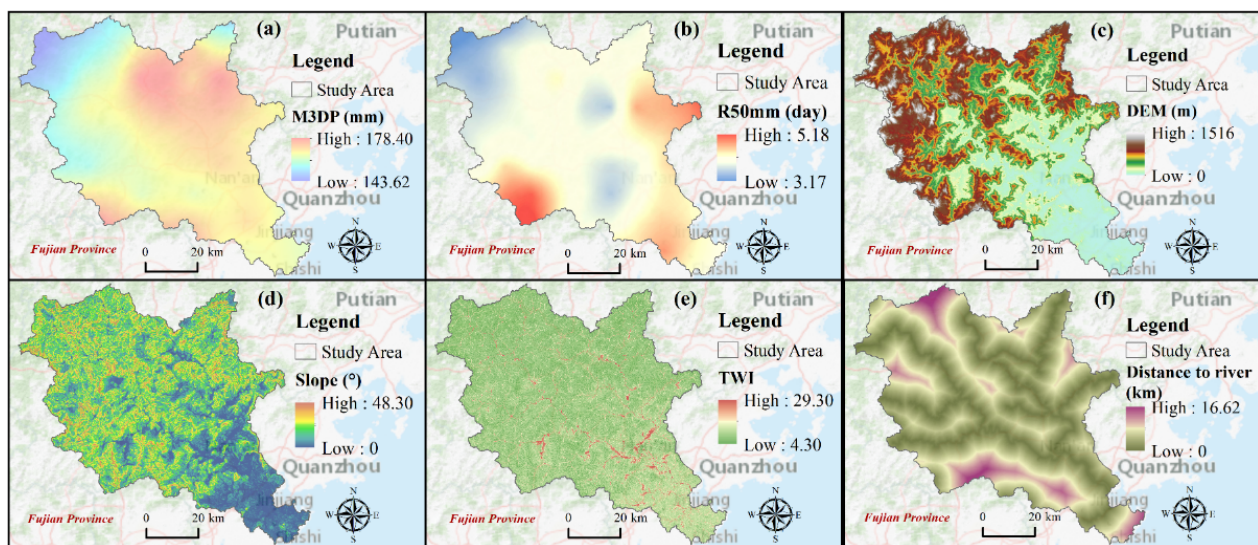


Figure 2. Disaster-inducing factors: (a) maximum three-day precipitation (M3DP), (b) number of days with daily rainfall ≥ 50 mm (R50 mm); disaster-breeding environments: (c) digital elevation model (DEM), (d) slope, (e) topographic wetness index (TWI), and (f) distance to river (DR).

The disaster-breeding environments considered five factors: digital elevation model (DEM), slope, distance to river (DR), topographic wetness index (TWI), and runoff coefficient (RC). The DEM (Figure 2c) represents the elevations of the Jinjiang Basin, which is inversely related to flood risk because of the flowing of water from higher elevations to lower elevations [40,41]. In this study, the DEM data were obtained from the Geospatial Data Cloud site, Computer Network Information Center, Chinese Academy of Sciences. As a factor can effectively reflect the degree of topographic undulations, slope is considered to influence flood genesis significantly [42]. Slope (Figure 2d) can directly affect the surface runoff and vertical percolation, which in turn affect the gathering of the water. Generally, areas with low slopes face a greater threat of flooding. In this study, slope was calculated by the DEM data using ArcGIS. The TWI (Figure 2e), reflecting the geotechnical wetness [43], is the accumulation of flow in any location in the basin. It is calculated using a function of slope and basin area, which is described in the study of Arora et al. [44]. Obviously,

when floods occur, areas along both banks of a river will be inundated. Therefore, the DR (Figure 2f) is an essential factor for assessing the flood risk in a specific area. The DR was estimated using the Euclidean distance [7]. The RC is another factor influencing the occurrence and process of floods [45], whose values are dependent on the land-use types to a large extent [46]. In this study, the RC was determined according to the Table 2, and varied with different land-use scenarios in 2030 and 2050.

Table 2. Land-use type and the corresponding runoff coefficient.

Land-Use Type	Cropland	Woodlands	Grassland	Water Area	Built-Up Land	Unused Land
Runoff coefficient	0.60	0.3	0.35	1.00	0.92	0.7

The hazard-bearing bodies used in this study included total population per unit area (POP, people/100 m²) and total general budget revenue per unit area (GBR, yuan/100 m²). The POP, a factor reflecting the social vulnerability [47], is considered to be very important for determining the flood risk [48]. The GBR was used to reflect the economic level of a unit, due to the strong correlation between it and Gross Domestic Product [49]. The raw datasets of these two factors were obtained from the Quanzhou statistical yearbook in 2020, and were spatialized using the spatialization model described in Section 3.3. Then, the POPs and GBRs of 2030 and 2050 were estimated according to the future land-use types and the topographic factors.

3. Methods

3.1. Land-Use Simulation Models

3.1.1. Markov Chain Model

The Markov chain model is essentially a stochastic process, which describes the possibility of one state changing to another state by a transition probability matrix [50]. Since the dynamic evolution of land use is characterized by Markov process [51], Markov model has been widely applied in predicting amounts of future land-use types, and has obtained high prediction accuracy. The Markov model can be expressed by the follow formula [52]:

$$S_{t+1} = P_{ij} \times S_t, \quad (1)$$

where S_t is the status of land-use types at the current time; S_{t+1} is the status of future land-use types, and P_{ij} represents the transition probability matrix for land-use types.

$$P = [P_{11} \cdots P_{1n} \cdots P_{n1} \cdots P_{nn}], \quad (2)$$

where $0 \leq P_{ij} \leq 1$, and $i, j = (1, 2, 3, \dots, n)$.

3.1.2. The FLUS Model and Accuracy Verification

The FLUS model was first proposed by Liu et al. in 2017, and is used to simulate the land-use changes [53]. The working mechanism of FLUS model integrates a bottom-up cellular automata (CA) and a deep learning algorithm—artificial neural networks (ANNs), and considers neighborhood influence, weight factors, self-adaptive land inertia, and conversion costs [13]. The integration of ANNs in FLUS model helps it to explore the nonlinear relationships between the driving factors and multiple land-use types more effectively [54]. In addition, the self-adaptive inertia mechanism and roulette selection mechanism of the FLUS model have been shown to be more effective for spatial simulation, compared with the traditional CA model [55]. Therefore, the FLUS model was considered to be better than CA and CLUE-S models, and has been applied in many studies [56–58].

In this context, the FLUS model was used in this study for the spatial simulation of land-use changes. First, the land uses were divided into six classes, according to the

land-use types in mainland China. Then, in order to obtain a probability distribution map, 14 driving factors and land-use data were used to train the ANNs model in FLUS model. As displayed in Figure S1 (Supporting Information), the 14 driving factors include the data on natural environment, social economy, and geographical location factors. Subsequently, based on the probability distribution map, the self-adaptive inertia mechanism and roulette selection mechanism of the FLUS model were used to simulate the land-use types in 2020 with the land use in 2010 as the starting year. Finally, Kappa test was applied to compare the simulation results in 2020 with the real 2020 land-use map, as follows [13]:

$$Kappa = (P_0 - P_c) / (P_p - P_c), \quad (3)$$

where P_0 is the correct proportion of the simulation; P_c is the correct proportion of the model in the random case, and P_p represents the proportion of the correct simulation in the case of ideal classification. From the verification results, we found that the kappa coefficient and overall accuracy reached 76.40% and 83.81%, respectively. These values showed that the accuracy of the simulation results were acceptable [53]. Therefore, the model was considered to be reliable and can be applied in future land-use simulation in 2030 and 2050.

3.2. Land-Use Simulation Scenario Setting

The direction of future land-use change cannot be fully determined [59]. In this context, many studies simulated the land-use change under different scenarios [60], such as natural growth scenario, ecological protection scenario, and urban expansion scenario [52]; low development scenario, medium development scenario, and high development scenario [61]. Considering the actual development of China and based on previous studies [62,63], three scenarios of natural growth scenario (NG), cropland protection scenario (CP), and ecological protection scenario (EP) were set in this study. According to the characteristics of each scenario model and with reference to the Master Plan for Land Use of Quanzhou and the Main Functional Zone Plan of Quanzhou, the demand area of each land type in each scenario was estimated by modifying the conversion probabilities of Markov chain model. More details of each scenario are described below.

The NG scenario was set to be consistent with the natural law of land-use type evolution in the study area, with an assumption that the land-use demand will not be affected by policy adjustments. Thus, under this scenario, the land-use demand was estimated only by the conversion probability matrix for the period 2000–2010, without any restrictions and adjustments.

The CP scenario was set to achieve the core goal of cropland protection, which is in accordance with the planning policy. In this scenario, the croplands were protected by restraining the expansion rate of built-up land and the conversion rates of cropland to other lands. Therefore, under the CP scenario, the conversion probabilities of croplands to built-up lands, woodlands, and water areas were reduced by 40%, 20%, and 20%, respectively, on the basis of the NG scenario.

The EP scenario was set to protect the ecological security, which is one of basic STATE policies in China. In this scenario, green mountains and green waters were protected (i.e., ecological lands such as woodlands and grasslands), and the conversion of ecological lands to built-up lands was strictly restricted. Therefore, under the EP scenario, the adjustments of conversion probabilities of croplands to other land types focused on (1) reducing the rate of conversion of croplands to built-up lands by 30% and adding the reduced part to the conversion of croplands to woodlands; (2) reducing the rate of conversion of both grasslands and woodlands to built-up lands by 50%.

After the scenarios were set up, the Markov chain model was used to estimate the land demand of each land-use type under the three scenarios (Table 3), with a step size of 10 years.

Table 3. The land demand of each land-use type under the three scenarios.

Year	Scenario	Cropland	Woodland	Grassland	Water Area	Built-Up Land	Unused Land
2020	/	173,528	250,238	75,297	6746	81,268	484
	NG	162,957	235,043	88,627	8364	91,944	623
2030	EP	162,957	243,227	89,995	8364	82,393	623
	CP	175,565	232,285	88,627	7974	82,485	623
	NG	134,735	212,102	108,011	11,322	120,543	848
2050	EP	146,668	230,356	114,399	10,673	84,592	873
	CP	179,905	201,947	109,825	9993	85,013	878

Unit: number of pixels.

3.3. Spatialization of Epigenetic Factors in Land Use

The spatial distributions of three deutero-genetic factors (i.e., RC, POP, and GBR) were obtained according to future land-use types. According to the previous study [6], the RC factor was spatialized based on the Table 2. For the POP and GBR variable, the spatial distributions of them were derived by constructing multiple linear regression models, according to the Quanzhou statistical yearbook in 2020. The multiple regression model has been widely used in studies on population spatialization, and has shown good performances [64,65]. In this study, in addition to the six land-use types, topographic factors (i.e., DEM, slope, and distance to river) were also taken into account in the regression modeling. These factors have been proven to have significant effects on the spatial distribution of the population [66]. Therefore, the general forms of the spatialized multiple regression model of POP and GBR in this study are as follows:

$$POP, GBR = \sum_{j=1}^n a_j x_j + \alpha \times DEM + \beta \times Slope + \delta \times DR + B_0 \tag{4}$$

where POP and GBR represent the total population and the total general budget revenue in a region, respectively; a_j is the regression coefficient of j_{th} land-use type; α , β , and δ are the regression coefficients of DEM, Slope, and DR (distance to river), and B_0 represents the intercept. In this study, the POP, GBR, land-use types, and topographic factors of 88 township-level administrative regions in this study area were used for regression modeling. Notably, according to the principle of no land, no population, the B_0 was set to 0.

However, the results of the POP and GBR simulations for the study area are necessarily in error with their real statistics. Therefore, in order to ensure that the simulated POP and GBR within the study area are equal to the actual statistical data, Equation (2) was used to adjust the model regression coefficients, thus making the model more reasonable.

$$\mu_i = \frac{p_r}{p_s} a_i, \tag{5}$$

where μ_i represents the adjusted regression coefficient of i_{th} variable; P_r is the real statistical values, and P_s is the simulated values for the study area. The adjusted spatialization models of POP and GBR in Jinjiang Basin are expressed as follows:

$$POP = 9.60 \cdot x_1 + 2.21 \cdot x_2 + 15.46 \cdot x_3 + 9.53 \cdot x_4 + 25.38 \cdot x_5 + 116.94 \cdot x_6 - 3.55 \cdot DEM - 2.29 \cdot Slope - 3.14 \cdot River \tag{6}$$

$$GBR = -6.62 \cdot x_1 - 6.03 \cdot x_2 + 0.56 \cdot x_3 + 24.41 \cdot x_4 + 23.58 \cdot x_5 + 38.76 \cdot x_6 + 5.03 \cdot DEM + 7.71 \cdot Slope + 0.06 \cdot River \tag{7}$$

where x_1 , x_2 , x_3 , x_4 , x_5 , and x_6 represent the croplands, woodlands, grasslands, water areas, built-up lands, and unused lands, respectively. The decision coefficients— R^2 —of the spatialization models of POP and GBR reached 0.867 and 0.530, respectively, which indicated that these two spatialization models had a good goodness of fit.

3.4. Flood Risk Determination Methods

3.4.1. Triangular Fuzzy Number-Based AHP (TFN-AHP)

Compared to the traditional AHP, the TFN-AHP applies the fuzzy set theory [67]. In applications, the TFN-AHP used triangular fuzzy numbers instead of the crisp numbers in the judgment structure matrix to express the importance degree between factors [68]. The triangular fuzzy number is defined as $P = (l, m, u)$, where the l and u represent the minimum and maximum possible values, while m is the most promising value [69]. The membership function of the $P = (l, m, u)$ is expressed as follows [70]:

$$\mu(x|\tilde{P}) = \begin{cases} 0 & \\ (x-l)/(m-l), l \leq x \leq m & \\ (u-x)/(u-m), m \leq x \leq u & \\ 0 & \end{cases} \quad (8)$$

The judgment matrix and the weights of factors determined by TFN-AHP are shown in Tables S2–S6 (Supporting Information), respectively.

3.4.2. Criteria Importance through Intercriteria Correlation (CRITIC)

The CRITIC, as a method of determining the objective weights, was proposed by Diakoulaki et al. in 1995 [71]. This method is conducted based on two concepts (i.e., the contrast intensity and the conflict in the decision criteria) [72]. The contrast intensity is represented by the standard deviation, which reflects the variable differences between classes. The larger the standard deviation, the greater the difference in variables between classes. The conflict in the decision criteria, which is based on the correlation between variables, decreases with increasing positive correlation of variables. Ultimately, the objective weighting of each factor is determined by a combination of contrast intensity and conflict. The conflict between the j th factor and other factors can be expressed as follows [6]:

$$\sum_{k=1}^n (1 - R_{kj}), \quad (9)$$

where R_{kj} represents the correlation coefficient between the k th factor and j th factor. Assuming that C_j denotes the amount of information contained in the j th factor, C_j can be expressed as follows:

$$C_j = S_j \sum_{k=1}^m (1 - R_{kj}), \quad (10)$$

where S_j is the standard deviation of the j th factor. Then, the weight of the j th variable can be calculated as follows:

$$W_j = C_j / \sum_j C_j, \quad (11)$$

In this study, the weights of factors determined by CRITIC are shown in Table S7 (Supporting Information).

3.4.3. Technique for Order Preference by Similarity to an Ideal Solution (TOPSIS)

The TOPSIS method, proposed by Hwang and Yoon et al. in 1981, attempts to address multi-attribute decision problems without articulation preference information representation [73]. This method is based on the concept that the ideal is the alternative with all the best values of attributes, while the negative ideal alternative has the worst levels of all attributes [30]. In fact, solving TOPSIS is a process that choosing alternatives that are simultaneously closest to the positive ideal and farthest from the negative ideal [74]. Thus, this technique can provide a cardinal ranking of the alternatives, based on the full use of attribute information. For more elaboration on the principles of the TOPSIS method, please refer to Yang et al. [34].

3.5. Processing

The workflow of dynamic assessment of the flood risk of Jinjiang Basin is illustrated in Figure 3. Firstly, the demand amount of land-use types was estimated using the Markov chain model according to the rules of scenarios setting (including NG, EP, and CP scenarios). Then, based on 14 driving factors, the FLUS model was applied to simulate the land-use changes. Further, based on the simulated land-use data, the RC was spatialized according to Table 2, and the future POPs and GBRs were spatialized by using the multiple regression models. Subsequently, based on the nine flood factors, the TFN-AHP and the hybrid model of CRITIC and TOPSIS were employed to generate a subjective flood risk result and an objective flood risk result of each year, respectively. Finally, the weighted average method was used to combine the above subjective and objective results to obtain the final flood risk map for each year under each scenario.

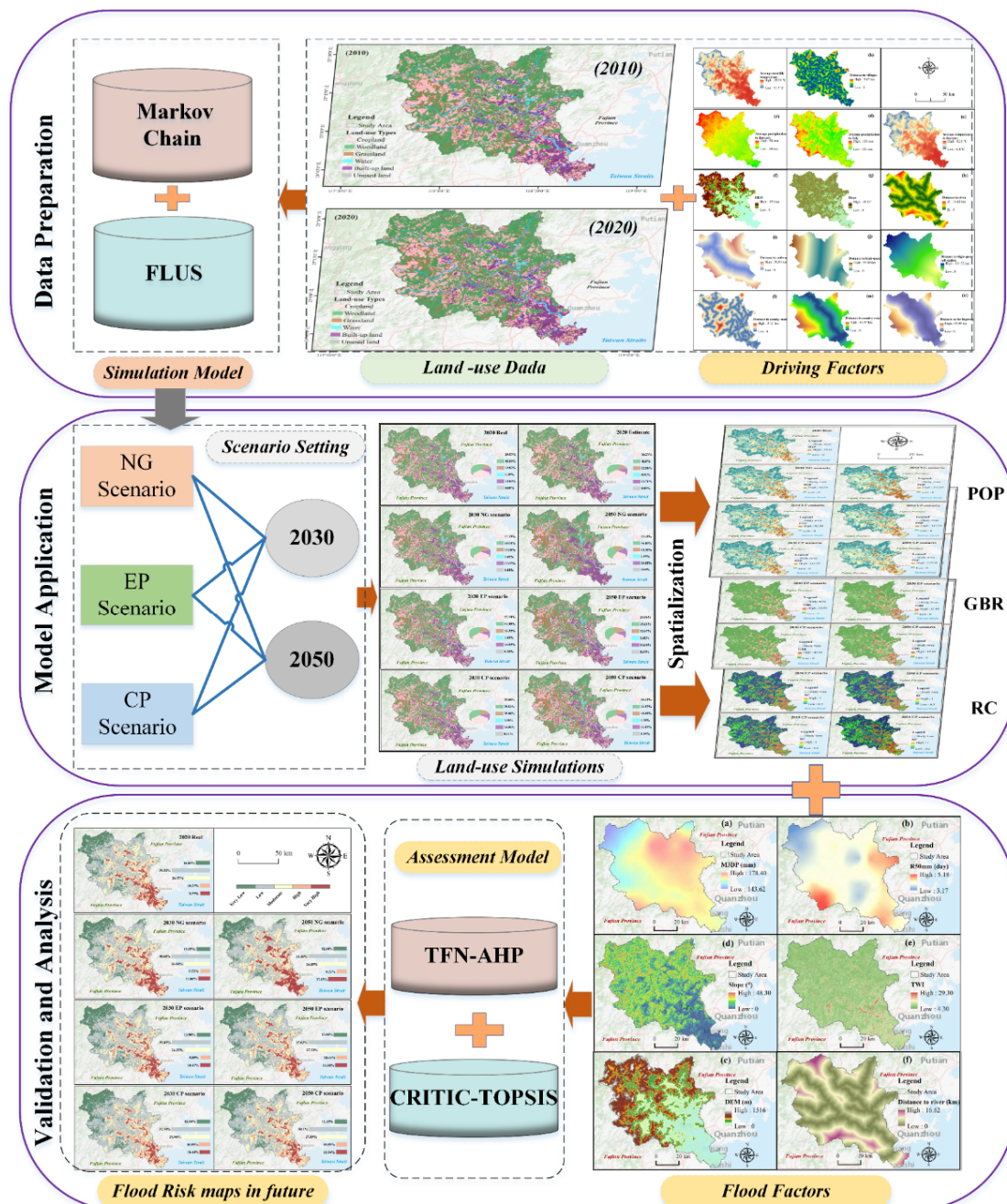


Figure 3. The workflow of dynamic assessment of the flood risk of Jinjiang Basin in this study.

4. Results

4.1. Land-Use Type Changes Based on Different Scenarios

Figure 4 depicts a quantified insight to the land-use changes, and Figure 5 shows the spatial distribution of future land-use types under the three scenarios. Notably, these quantitative comparisons are based on the situation of 2020. In the NG scenario of 2030, the areas of grasslands, water areas, and built-up lands will increase by 2.27%, 0.27%, and 1.82%, respectively. By 2050, these values will reach 5.57%, 0.78%, and 6.68%, respectively. However, apparent downward trends in areas of the croplands and the woodlands will be detected, with decreases of 1.80% and 2.58% in 2030, and 6.60% and 6.49% in 2050. Under the EP scenario, by 2030, the grasslands will increase the most (2.50%), followed by water areas (0.27%) and built-up lands (0.19%). This ranking is also reflected in the EP scenario of 2050, with proportions of increase in grasslands, water areas, and built-up lands reaching 4.15%, 0.39%, and 0.37%, respectively. The croplands and the woodlands, however, presented slightly decreased areas. From 2020 to 2030, they will decline by 1.80% and 1.19%, respectively, and will decline 2.78% and 2.19% by 2050, respectively. Under the CP scenario, only the woodlands will reduce over 2020–2050, while the other five land-use types all show upward trends. In this scenario, woodlands will decline by 3.05% and 8.21% in 2030 and 2050, respectively. On the contrary, the croplands, grasslands, water areas, built-up lands, and unused lands will increase by 0.35%, 2.27%, 0.20%, 0.21%, and 0.02%, respectively, by 2030. These values will be 1.09%, 5.88%, 0.55%, 0.64%, and 0.07%, respectively, by 2050.

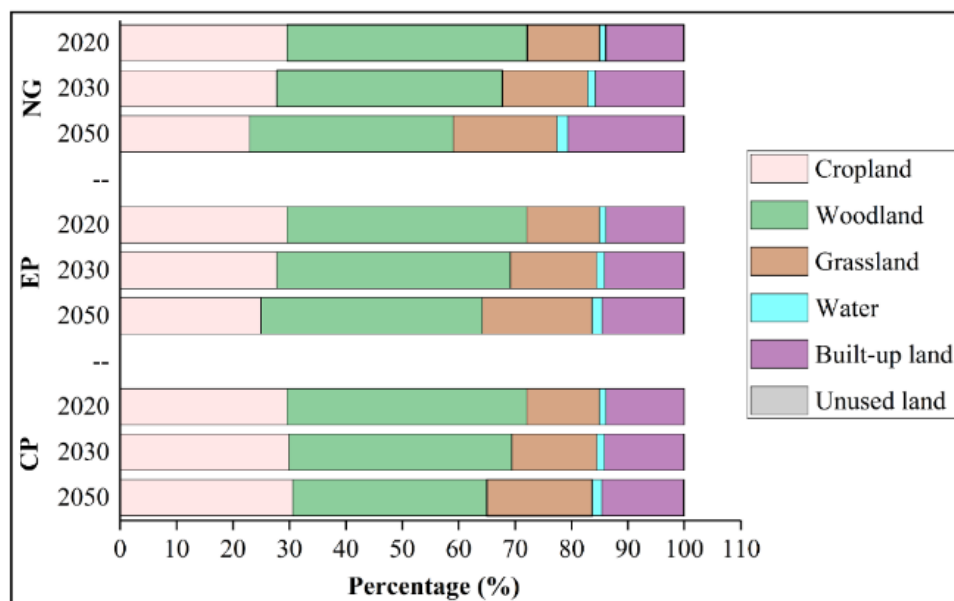


Figure 4. The area changes of future land-use types under the scenarios of natural growth scenario (NG), cropland protection scenario (CP), and ecological protection scenario (EP) in 2030 and 2050, compared to 2020.

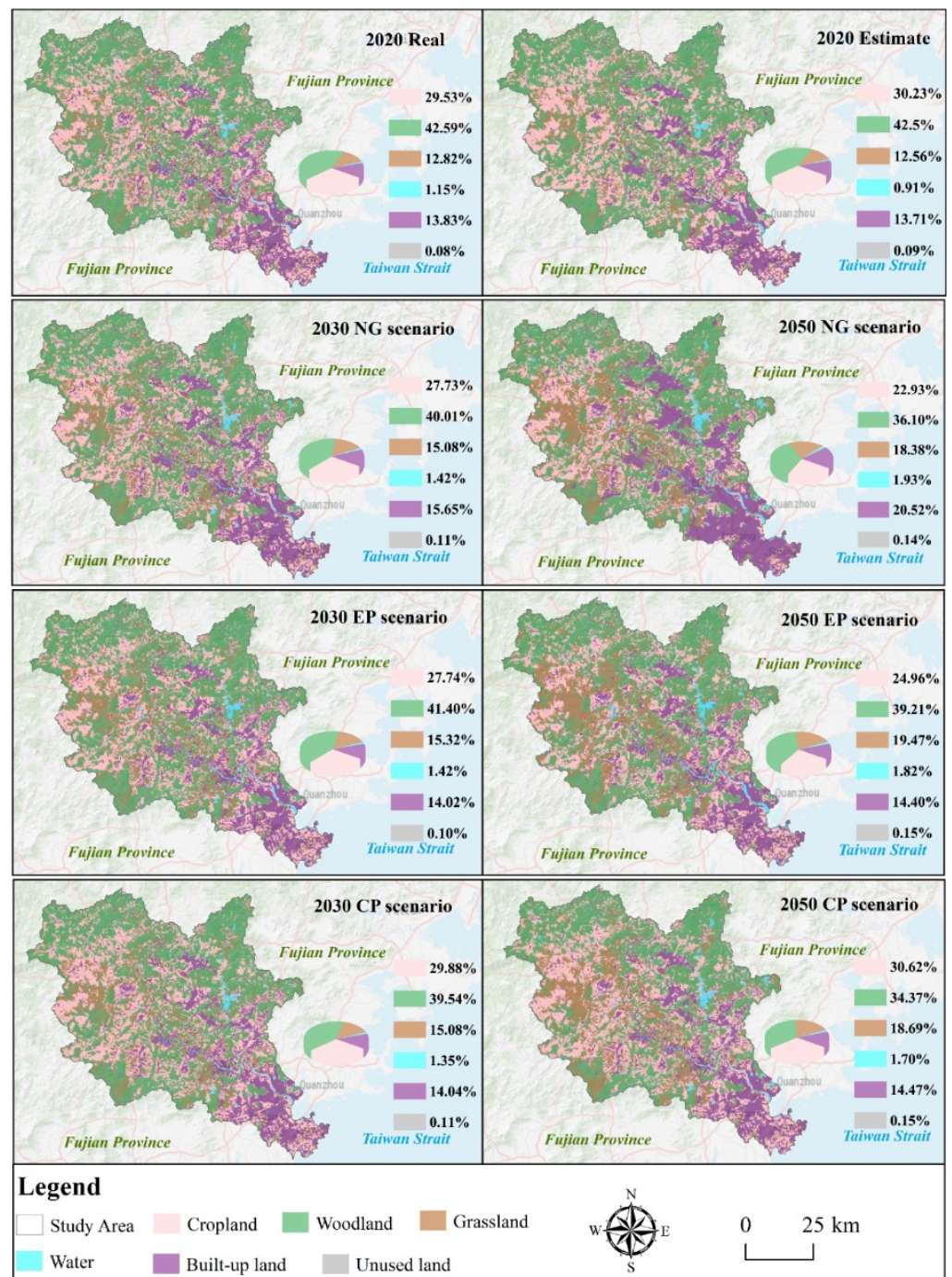


Figure 5. Land-use simulation results under the three scenarios in 2030 and 2050.

4.2. The Spatialization Results of the Epigenetic Variables

The spatialization results of RC, POP, and GBR under the three scenarios are presented in Figures 6–8, and Table 4 shows the quantified changes of POP and GBR. Under the NG scenario, the total POP of Jinjiang Basin will increase from 4.23 million people in 2020 to 4.68 million people in 2030 and 5.44 million people in 2050. The average annual growth rate of total POP in this scenario will reach 1.27% over 2020–2050. For the GBR in the NG scenario, it maintains an average annual growth rate of 4.46% over 2020–2050, and the total GBR of the region will reach 33.20 billion yuan by 2050. Compared to the NG scenario, a lower rate of population and economic growth can be found under the EP scenario. In this scenario, by 2050, the total POP and GBR of Jinjiang Basin will be 4.78 million people and

23.43 billion yuan, respectively, with an average annual growth rate of 0.61% and 2.66%, respectively. Similar to the EP scenario, both the population and the economy growth rates in the CP scenario will be also slower than those in the NG scenario. By 2050, the total POP of the basin will reach 4.97 million people, while the GBR of this basin will be 23.07 billion yuan. The average annual growth rate of total POP and GBR in the CP scenario will become 0.80% and 2.58%, respectively. Spatially, the densely populated and economically developed areas are consistently distributed and are mainly located on built-up lands.

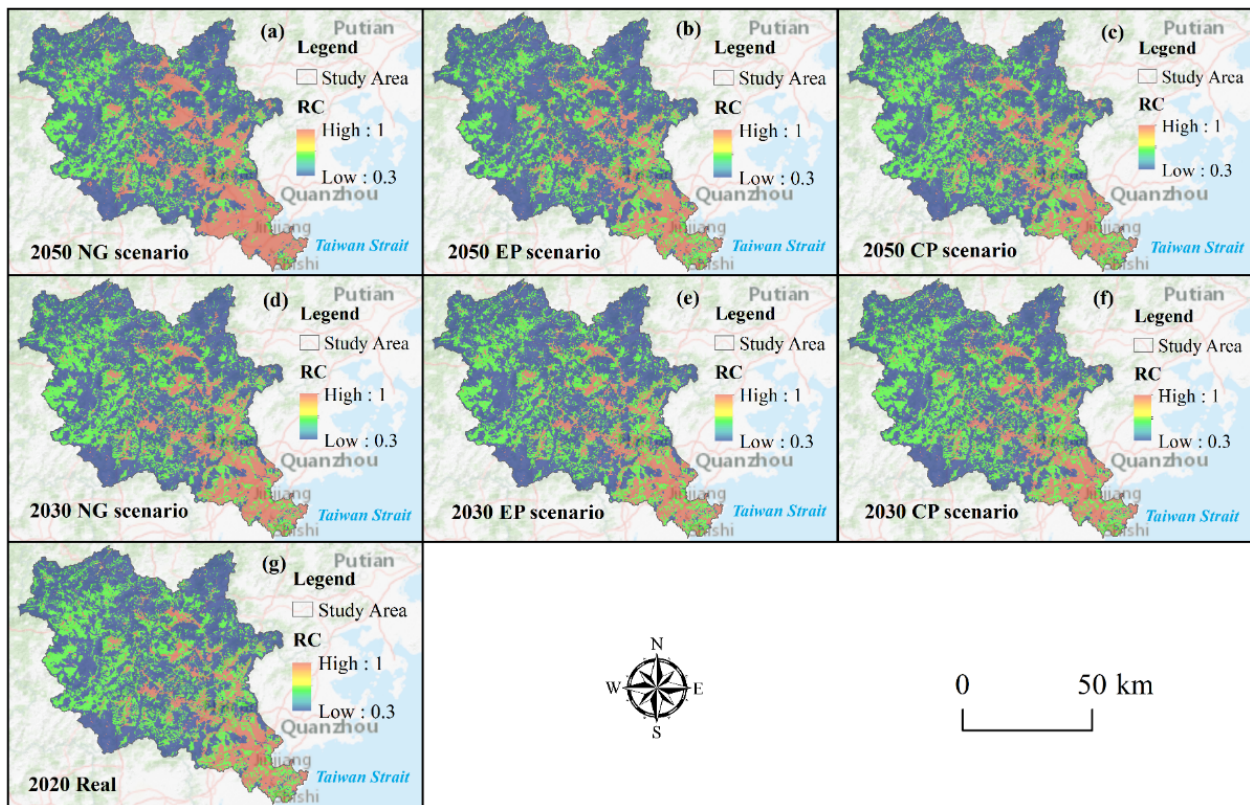


Figure 6. Spatial distribution of future runoff coefficient (RC) in 2030 and 2050. NG, EP, and CP scenarios represent natural growth, ecological protection, and cropland protection scenarios, respectively. Subfigures (a), (b) and (c) are the RCs under NG, EP and CP scenarios in 2050, respectively. Subfigures (d), (e) and (f) are the RCs under NG, EP and CP scenarios in 2030, respectively. Subfigures g is the RC in 2020.

Table 4. The total POP and GBR in the Jinjiang Basin under the three scenarios from 2020 to 2050. AAGR represents the average annual growth rate starting in 2020.

Variables	2020	2030			2050		
		NG	EP	CP	NG	EP	CP
POP	4.23	4.68	4.48	4.55	5.44	4.78	4.97
AAGR	/	1.02%	0.57%	0.73%	1.27%	0.61%	0.80%
GBR	13.86	23.18	20.67	20.50	33.20	23.43	23.07
AAGR	/	5.28%	4.08%	3.99%	4.46%	2.66%	2.58%

POP is the population, whose unit is set as million people; GBR is the general budget revenue, whose unit is set as billion yuan.

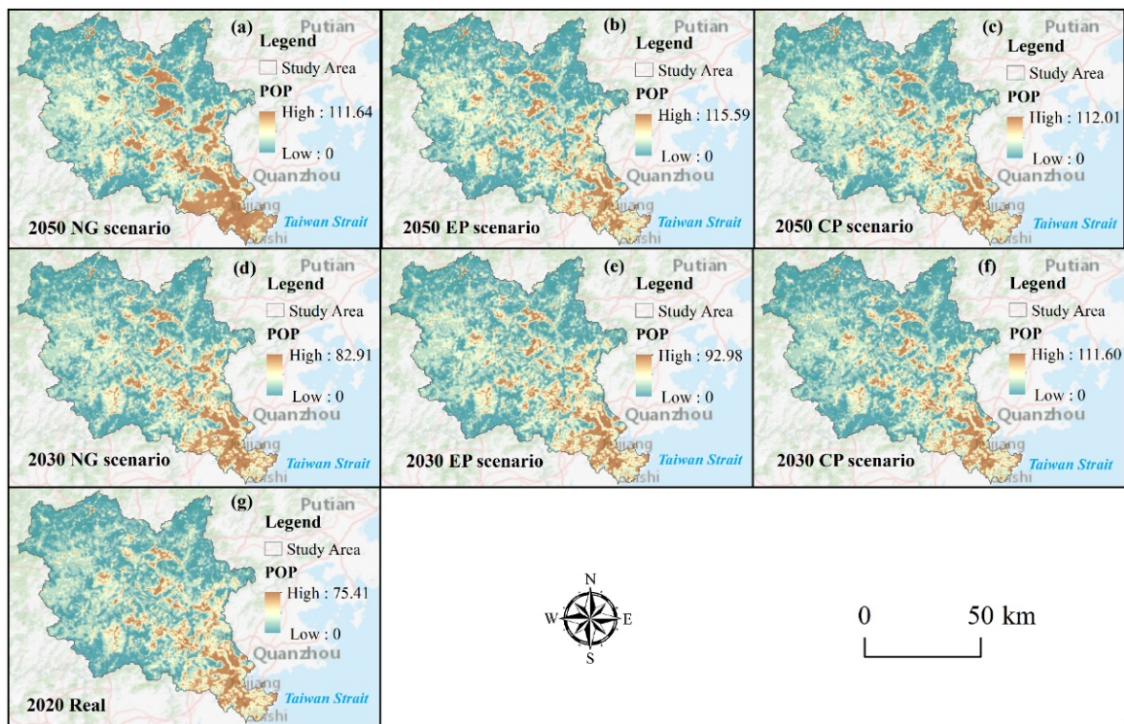


Figure 7. Spatial distribution of future population (POP, million people/100 m²) in Jinjiang Basin. NG, EP, and CP scenarios represent natural growth, ecological protection, and cropland protection scenarios, respectively. Subfigures (a), (b) and (c) are the POPs under NG, EP and CP scenarios in 2050, respectively. Subfigures (d), (e) and (f) are the POPs under NG, EP and CP scenarios in 2030, respectively. Subfigures g is the POP in 2020.

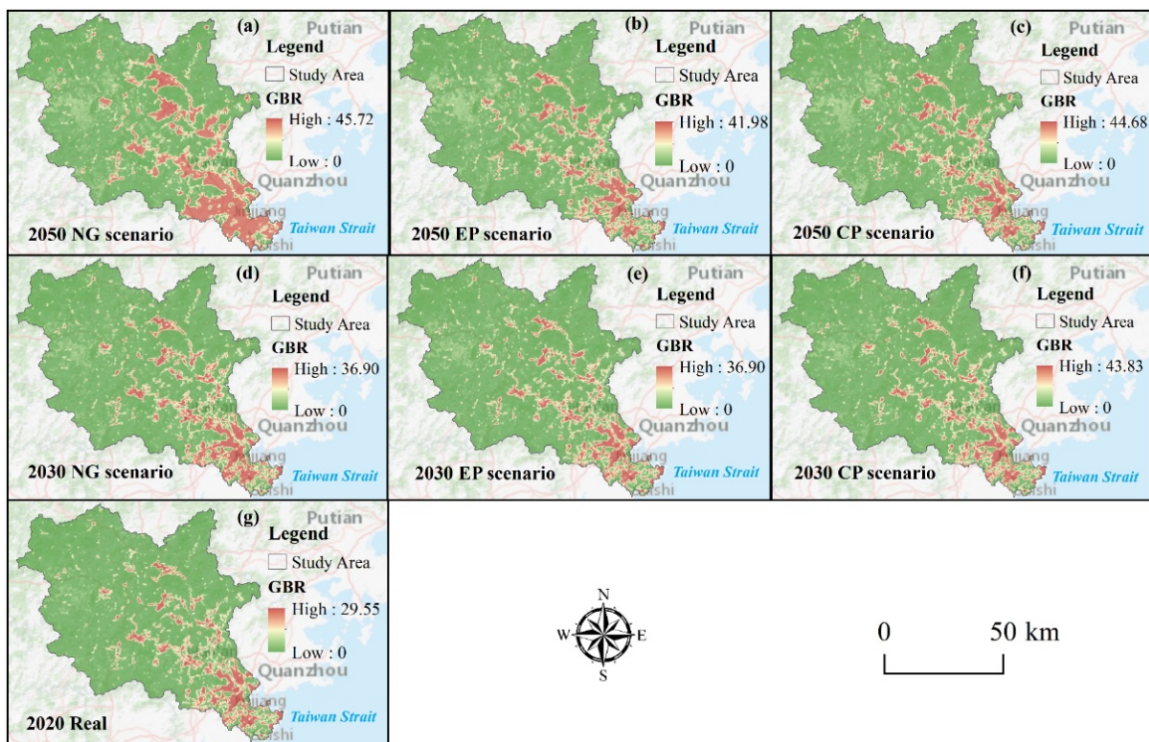


Figure 8. Spatial distribution of future general budget revenue per unit area (GBR, billion yuan/100 m²) in Jinjiang Basin. NG, EP, and CP scenarios represent natural growth, ecological protection, and cropland protection scenarios, respectively. Subfigures (a), (b) and (c) are the GBRs under NG, EP and CP scenarios in 2050, respectively. Subfigures (d), (e) and (f) are the GBRs under NG, EP and CP scenarios in 2030, respectively. Subfigures g is the GBR in 2020.

4.3. Spatio-Temporal Characteristics of Future Flood Risk

4.3.1. Temporal Patterns of the Flood Risk

Figure 9 shows the spatial distributions of future flood risks and the statistical results of each risk level in 2030 and 2050. Under the NG scenario, there is a substantial decrease in the area of the low-flood-risk class and a significant increase in the area of the high-flood-risk class over 2020–2050. By 2030, the total area of low and very low risk levels will decline 85.60 km², while that of high and very high risk levels will increase by 91.24 km², compared to 2020. By 2050, the total area of very low and low risk levels will decline by 364.20 km², and the total area of very high and high risk levels will increase by 371.30 km². Therefore, if the Jinjiang Basin develops according to the NG scenario, the flood risk of the area will grow significantly.

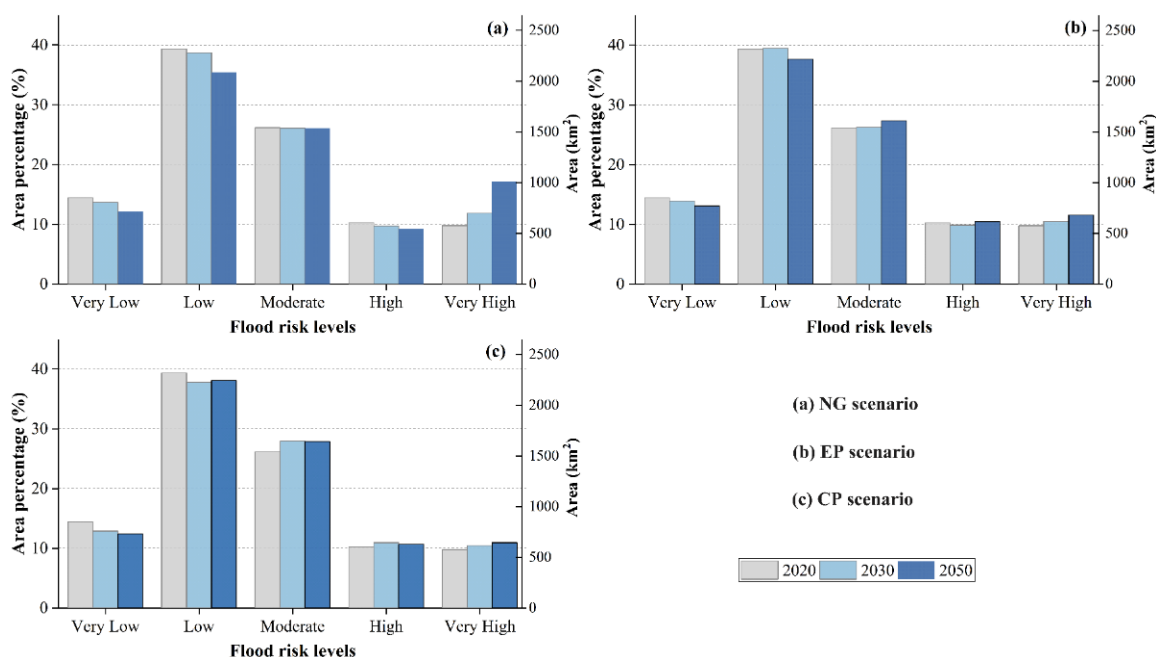


Figure 9. Changes of future flood risk under the natural growth scenario (NG), cropland protectable 2030 to 2050 in Jinjiang Basin.

Under the EP scenario, the areas of the five risk levels in the years of 2030 and 2050 were similar to those in 2020, with only minor changes. Compared to 2020, the total area of very low and low risk levels in 2030 and 2050 will decrease by 23.46 km² (0.40%) and 180.81 km² (3.08%), respectively. The total area of very high and high risk levels will increase by only 19.18 km² (0.33%) by 2030 and 113.75 km² (1.94%) by 2050, compared to 2020. Obviously, the degree of flood risk in Jinjiang Basin under the EP scenario will not change a lot, indicating that the flood risk in the area is well controlled.

The areas of the flood risk levels under the CP scenario in 2030 and 2050, similar to the EP scenario, do not change significantly compared to those of 2020. Under this scenario, the total area of very low and low risk levels in 2030 and 2050 will decrease by 183.56 km² (3.12%) and 191.87 km² (3.27%), respectively. The total area of very high and high risk levels will increase by only 79.6 km² (1.35%) by 2030 and 90.96 km² (1.55%) by 2050, compared to 2020. From the above changes, it can be seen that the CP scenario effectively avoids further aggravation of flood risk in Jinjiang Basin.

4.3.2. Spatial Patterns of the Flood Risk

Figure 10 is the conversion map of flood risk from 2020 to 2050 in Jinjiang Basin, which reveals the locations where flood risk will increase or decline. From this map, we can see that the increased flood risk in future mainly occurs in the periphery of existing built-up

lands. Figure 11 presents the spatial distribution of future flood risk under three scenarios in the study area. It can be seen from Figure 11 that there is a clear regional variation of flood risk in this area, decreasing from southeast to northwest. The zones characterized by high and very high flood risk levels are mainly distributed in the southeast of the Jinjiang Basin, while the low and very low zones are mainly located in the northwest of this study area. In addition, these high-flood-risk areas can also be found near the main stream in Jinjiang Basin.

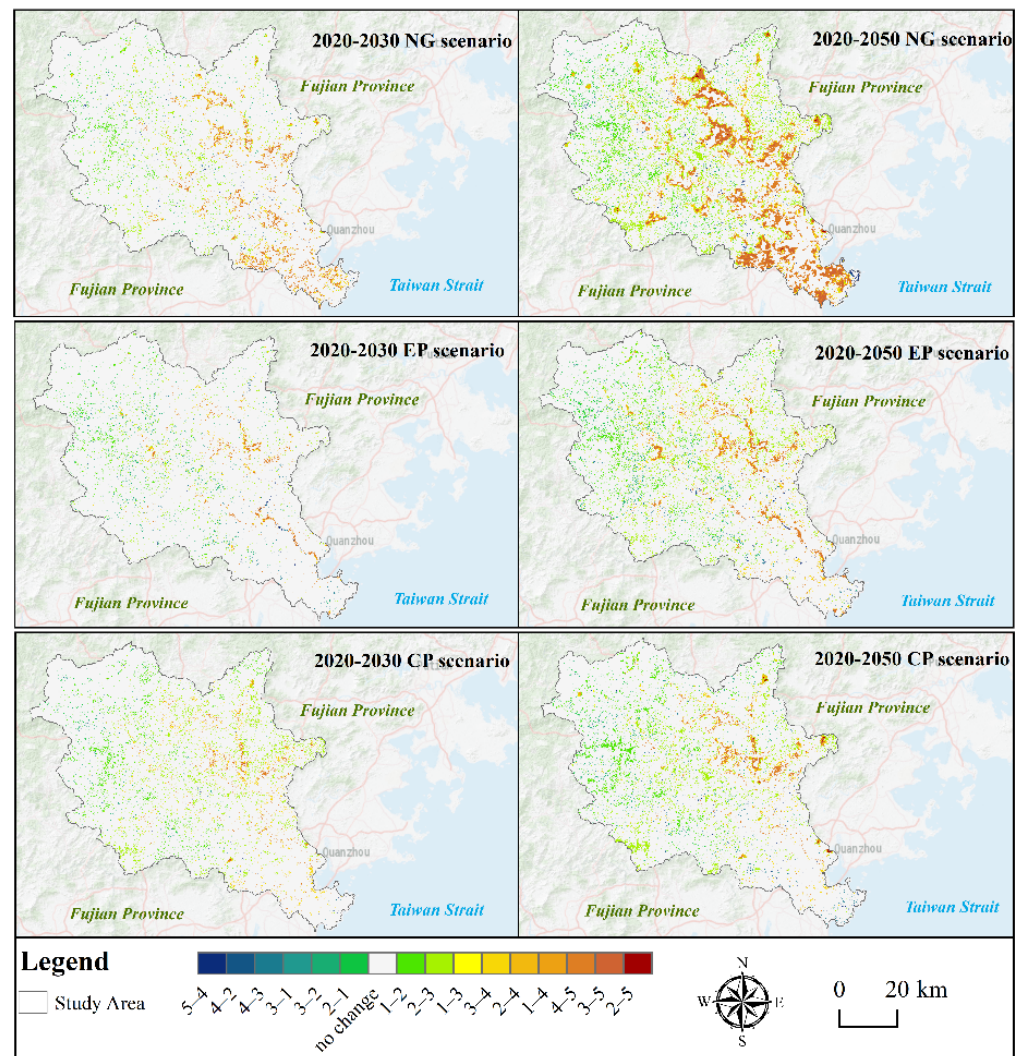


Figure 10. Dynamic changes in flood risk levels under three scenarios from 2020 to 2050 in the Jinjiang Basin. The Roman numerals from 1 to 5 represent very low, low, moderate, high, and very high, respectively. The Roman numeral on the left of “—” represents the flood risk level of 2020, while that on the right represents the year 2030 or 2050. NG, EP, and CP scenarios represent natural growth, ecological protection, and cropland protection scenarios, respectively.

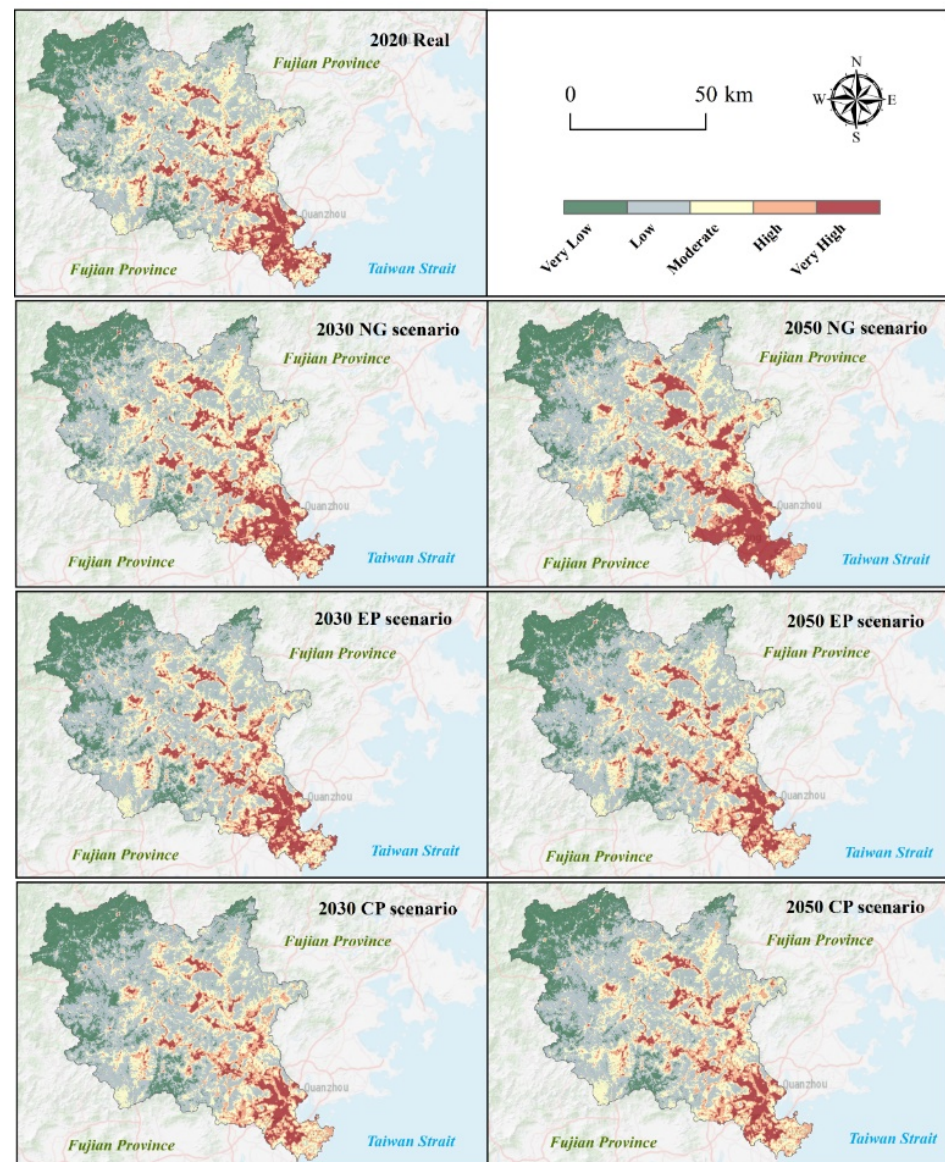


Figure 11. The future flood risk maps under the three scenarios from 2030 to 2050 in Jinjiang Basin. NG, EP, and CP scenarios represent natural growth, ecological protection, and cropland protection scenarios, respectively.

5. Discussion

5.1. Analysis of Simulation Results

By applying the proposed framework in the data of Jinjiang Basin, it is found that the simulation results under the three scenarios are different. In the NG scenario, urban expansion is fastest, with a 6.82% increase in built-up lands by 2050. This expansion comes at the expense of other less profitable land uses (i.e., croplands and woodlands, which will decline by 6.60% and 6.49% by 2050, respectively). Meanwhile, this expansion is also a manifestation of increased human interference and urbanization as well as the main attributes of the changes in the land-use pattern [75,76]. From a spatial perspective, the urban expansion mainly occurs in the periphery of almost all of the existing conurbation. In this context of rapid urbanization, demand for urban built-up land, such as transportation land, residential land, recreational facility land, and industrial production land, will increase, due to the flow of migrant workers into the city [77]. Among which, the increasing of industrial production land can provide more employment opportunities for people, which further promote growth in population size and economic aggregates [78]. As expected,

the POP and GBR under the NG scenario will increase rapidly, with an average annual growth rate of 1.27% and 4.46% from 2020 to 2050. The growths in POP and GBR directly increase the exposed populations and assets to flooding, thus leading to an increase in flood vulnerability. However, due to the unplanned growth, there is pressure on land, housing, infrastructures, and the environment. Thus, it is difficult for infrastructure to keep pace with this unplanned urbanized growth [76]. Then, the increase of flood vulnerability will contribute to the higher risk of flooding. On the other hand, the decreasing woodlands and increasing built-up lands result in the increase of RC, which in turn leads to the heightened flood risk. As Liu et al. point out, such land-use changes can result in an increase of peaking flows and the changes in rainfall–runoff processes [12]. Overall, vegetative surface being removed, raw lands being replaced by impervious pavements, and the increased exposure of POP and economy, because of the urbanized growth, have been the main reasons for the flood risk increase in the NG scenario. Obviously, flood risk in this scenario is severe, with a total increase of 371.30 km² in the very high and high risk levels by 2050. Therefore, the current land-use system (NG scenario) is considered to be unsustainable in the long term.

In the EP scenario, the woodlands will be protected effectively, with a decline of only 1.19% by 2030, and only 2.19% by 2050. At the same time, urban expansion slows down significantly, with an increase in built-up lands of approximately only 0.37% noted in the region. However, compared with the other two scenarios, this rate is significantly lower. The slow urban expansion directly reveals the phenomenon of slowing population and economic growth in this scenario. This is because the balance between socio-economic development and ecological protection in the EP scenario results in lower population and economic growth [79]. According to Table 4, the average annual growth rates of POP and GBR will only become 0.61% and 2.66% over 2020–2050, respectively. This means that no significant increase in flood vulnerability will occur. Further, the values of RC in the study area also will not change significantly due to small reductions in woodlands and built-up lands. The above two aspects can explain the fact that no significant increase in flood risk occurs under the EP scenario. Interestingly, under the EP scenario, it can be found that the flood risk level of large areas far away from the built-up land changes from high to low (Figure 10). This finding confirms the effectiveness of ecological conservation policies in mitigating increased flood risk. As highlighted by Villarreal-Rosas et al. for some local government areas and beneficiaries, changes in flood protection were also driven by increases in forest cover or spatial changes in demand [80]. In addition, most increased flood risk in this scenario can be found in the northeast of the study area and along the Jinjiang River, which is different from that in NG scenario (Figure 10). This may be due to the fact that in the southeastern part of the study area, which is more developed, there is little suitable space for urban expansion under the constraints of ecological protection guidelines. However, in the northeastern part of the study area, where development is relatively slow, there are more areas that are suitable for development without violating ecological protection principles. As a result, most of the urban expansion will occur here in the EP scenario (Figure 5), which leads to an increased risk of flooding. In summary, the risk level of flooding tends to stabilize under the EP scenario, with only a small increase in flood risk in the northeastern part of the study area. Therefore, the EP development pattern is preferred.

In the CP scenario, the loss of croplands will have been effectively stopped and the croplands area will increase. By 2030, the areas of croplands will increase 0.35%, and will increase 1.09% by 2050, compared to 2020. However, there is a significant decline in the area of woodlands, with a decrease of 8.21% by 2050, which may be attributed to the reclaiming of woodlands. At the same time, the rate of urban expansion will slow down significantly, with an increase of only 0.21% by 2030 and 0.64% by 2050, with an accompanying moderate population and economic growth. According to Table 4, the average annual growth rate of total POP and GBR in the CP scenario will become only 0.80% and 2.58%, respectively. Thus, the vulnerability of flood will not increase substantially. This in turn leads to no significant increase in flood risk over 2020–2050 in the CP scenario. According to Figure 9,

the total area of very high and high risk levels will increase by only 90.96 km² (1.55%) by 2050, compared to 2020. Similar to the EP scenario, these small increases in flood risk are also mainly distributed in the northeastern part of the study area. From the perspective of flood risk management, the CP scenario is advantageous.

5.2. Applications and Uncertainty of the Framework

To assess future flood risk reliably, a complex framework has to be applied, including the linkage of future land-use simulation with spatialization technology of factor and flood risk determination models. Furthermore, the socio-economic developments associated with the future land-use changes under different scenarios have been considered in this framework. Consequently, the deep uncertainty related to future dynamic changes in the social development can be considered. This framework also provides a new idea for the flood risk assessment at a basin scale, which reveals the dynamic changes of flood risk at a spatio-temporal scale from future perspectives. The results under this framework application are helpful for decision-makers to understand future flood characteristics and verify the adequacy of current flood response measures. According to the differences in the flood risk under future development pathways, policies can be given greater flexibility, thus avoiding as much as possible nonessential flood prevention and the limiting of economic development. This can be achieved by depicting plausible, potentially coherent, and internally consistent storylines of different socioeconomic trajectories [81].

Uncertainties of the study are very essential as this is a new approach to assess the future flood risk with respect to land-use changes [59]. To begin with, accurately simulating the future land-use types is a challenging task because of the inherent uncertainty of a future land-use model [82]. Considering that the number of potential futures is actually infinite, predicting the future in a precise manner is less realistic [83]. In this context, the purpose of determining the future flood risk under the different land-use scenarios is to explore possible future directions and to consider a range of alternative pathways [84]. In addition, another important driver for future flood risk is economic development, considered by adjusted POP and GBR values [85]. These adjusted POP and GBR values were predicted in this study by spatialization technology (a multiple linear regression model), according to the land-use types and topographic factors. However, we cannot currently take into account all the factors that affect future socio-economic development, such as investments for technical improvements [85]. Consequently, the projected POP and GBR values in this study have a small deviation from the real value, which can be reflected by comparing their average annual growth rates in the past 10 years (2010–2020) with that in the future NG scenario. According to the Quanzhou statistical yearbook and Table 4, the average annual growth rate of GBR during 2010–2020 is 7.68%, while in NG scenario, the average annual growth rate of GBR from 2020 to 2030 is only 5.28%. For the POP values, the average annual growth rate of POP in 2010–2020 is 1.05%, while in NG scenario from 2020–2030, it is 1.02%. Therefore, the spatialization model's calibration and optimization could be further improved, although the internal spatial diversity of POP and GBR has been quantified by these models. On the other hand, most studies have shown that land-use changes have a direct impact on the runoff, peak flow and hydrograph [86–88]. However, due to the data availability limitations, our approach required a simplifying assumption. In this study, the six land-use types are distinguished with RC values ranging from 0.6 to 1 (Table 2) [6], as a flood conditioning factor to reflect the impact of land-use changes on runoff (Figure 6). As a multicriteria decision assessment method, this quantification ignores the spatial heterogeneity of RC within a particular land-use type, and also cannot reflect other hydrological factors, such as peak flow.

In addition to the uncertainties, our study also highlights several limitations. Since the purpose of this study is to propose a framework and explore the dynamics of flood risk, not to predict future land-use changes, there is no focus on the driving causes of land-use changes. The land-use simulation was based on the current state without considering the changes of information such as traffic in the future. In addition, future flood risk

management has not been taken into this framework, which may lead to an overestimation of flood risk [13]. Moreover, future climate change factors are suggested to be taken into account for a more realistic flood risk simulation in future studies.

6. Conclusions

By considering the effects of land-use changes, a dynamic future flood risk assessment framework was proposed in this study, and applied in data from Jinjiang Basin. In the construction of this framework, computational scenario-based land-use changes in 2030 and 2050 were simulated by FLUS model first. Subsequently, based on the connections established among the POP and GBR with land-use types and topographic factors, multiple linear regression was introduced to capture interior spatial distribution of POP and GBR, thus replacing a lumped/overall value. Finally, on the basis of the spatialization results and seven flood conditioning factors, future flood risk maps under three scenarios were generated by the TFN-AHP and the novel hybrid model (CRITIC-TOPSIS). These results of the framework application reveal the spatio-temporal changes of flood risk in Jinjiang Basin under the three scenarios.

Overall, an increase of flood risk in the future is expected to occur Jinjiang Basin, but the magnitude of the increase varies under the three scenarios. In the NG scenario, built-up lands expand rapidly, whose area increases by 6.68% by 2050. The population and economy maintain high growth rates, with an average annual growth rate of 1.27% and 4.46%, respectively. In this scenario, the total area of very high and high flood risk levels increases by 371.30 km² by 2050, while that of very low and low flood risk levels declines by 364.20 km². In the EP scenario, woodlands will be protected effectively, with a decline of only 2.19% by 2050. However, the area of built-up lands increases by only 0.37%, and the POP and GBR increase at average annual growth rates of only 0.61% and 2.66%, respectively. The total area of very high and high flood risk levels will increase by only 113.75 km² by 2050. In the CP scenario, the loss of croplands will have been effectively stopped, with an increase by 1.09% by 2050. Similar to the EP scenario, the rates of urban expansion, population, and economic growth will slow down significantly in this scenario. There is also no significant increase in total area of very high and high flood risk levels, with an increase by only 90.96 km² by 2050. It was also found that the high and very high flood risk zones are mainly distributed in the southeast of the Jinjiang Basin and scattered near the main river channels. The increased risk of flooding mainly occurs in the periphery of existing conurbation. This flood risk information determined by the proposed framework provides an insight into the spatial distribution of future flood-prone areas in the region. In future studies, the impact of climate change as well as future flood management measures deserve to be taken into account.

Supplementary Materials: The following are available online at <https://www.mdpi.com/article/10.3390/w13223239/s1>, Figure S1: Spatial distribution characteristic of each driving factor of land-use changes, Table S1: The overview of data used in the future land-use simulation, Table S2: Parameters of disaster-inducing factors, disaster-breeding environments, and hazard-bearing bodies in the triangular fuzzy number-based AHP (TFN-AHP), Table S3: Parameters of disaster-inducing factors in the triangular fuzzy number-based AHP (TFN-AHP), Table S4: Parameters of disaster-breeding environments in the triangular fuzzy number-based AHP (TFN-AHP), Table S5: Parameters of hazard-bearing bodies in the triangular fuzzy number-based AHP (TFN-AHP), Table S6: The weights of each factor determined by triangular fuzzy number-based AHP (TFN-AHP), Table S7: The weights of each factor determined by criteria importance through intercriteria correlation (CRITIC).

Author Contributions: Conceptualization, J.L. and J.X.; methodology, J.L. and J.W.; software, X.C. and W.C.; validation, J.L. and W.H.; formal analysis, Y.H.; investigation, G.Y.; resources, N.W.; data curation, J.L.; writing—original draft preparation, J.L.; writing—review and editing, J.W. and Y.D.; visualization, J.X.; supervision, J.W. and J.X.; project administration, J.W.; funding acquisition, J.X. All authors have read and agreed to the published version of the manuscript.

Funding: This paper is supported by Key R & D project of Sichuan Science and Technology Department (Grant No. 2021YFQ0042), Key R & D project of Sichuan Science and Technology Department (Grant No. 21QYCX0016), National Key R&D Program of China (2020YFD1100701), Strategic Priority Research Program of the Chinese Academy of Sciences (Grant No. XDA20030302), and the Science and Technology Project of Xizang Autonomous Region (Grant No. XZ201901-GA-07), National Flash Flood Investigation and Evaluation Project (Grant No. SHZH-IWHR-57), Project from Science and Technology Bureau of Altay Region in Yili Kazak Autonomous Prefecture (Grant No. Y99M4600AL). The authors are grateful to this support.

Institutional Review Board Statement: Not applicable.

Informed Consent Statement: Not applicable.

Data Availability Statement: Precipitation data (GPM) are available at https://disc.gsfc.nasa.gov/datasets/GPM_3IMERGDE_06/summary?keywords=GPM (accessed on 18 April 2021). DEM data are available at <https://srtm.csi.cgiar.org/srtmdata/> (accessed on 6 May 2021). Land-use data are available at <http://www.globeland30.com> (accessed on 20 May 2021). The Quanzhou statistical yearbook is available at <http://tj.quanzhou.gov.cn/tjzl/tjsj/ndsjs/> (accessed on 1 June 2021). River data are available at the National Flash Flood Investigation and Evaluation Project.

Conflicts of Interest: The authors declare no conflict of interest.

References

- Hong, H.Y.; Tsangaratos, P.; Ilia, I.; Liu, J.Z.; Zhu, A.X.; Chen, W. Application of fuzzy weight of evidence and data mining techniques in construction of flood susceptibility map of Poyang County, China. *Sci. Total Environ.* **2018**, *625*, 575–588. [[CrossRef](#)] [[PubMed](#)]
- Dano, U.L.; Balogun, A.L.; Matori, A.N.; Yusouf, K.W.; Abubakar, I.R.; Mohamed, M.A.S.; Aina, Y.A.; Pradhan, B. Flood Susceptibility Mapping Using GIS-Based Analytic Network Process: A Case Study of Perlis, Malaysia. *Water* **2019**, *11*, 615. [[CrossRef](#)]
- Khosravi, K.; Nohani, E.; Maroufinia, E.; Pourghasemi, H.R. A GIS-based flood susceptibility assessment and its mapping in Iran: A comparison between frequency ratio and weights-of-evidence bivariate statistical models with multi-criteria decision-making technique. *Nat. Hazards* **2016**, *83*, 947–987. [[CrossRef](#)]
- Leskens, J.G.; Brugnach, M.; Hoekstra, A.Y.; Schuurmans, W. Why are decisions in flood disaster management so poorly supported by information from flood models? *Environ. Model. Softw.* **2014**, *53*, 53–61. [[CrossRef](#)]
- Yu, F.L.; Chen, Z.Y.; Ren, X.Y.; Yang, G.F. Analysis of historical floods on the Yangtze River, China: Characteristics and explanations. *Geomorphology* **2009**, *113*, 210–216. [[CrossRef](#)]
- Lai, C.G.; Chen, X.H.; Wang, Z.L.; Yu, H.J.; Bai, X.Y. Flood Risk Assessment and Regionalization from Past and Future Perspectives at Basin Scale. *Risk Anal.* **2020**, *40*, 1399–1417. [[CrossRef](#)]
- Costache, R.; Pham, Q.B.; Avand, M.; Linh, N.T.T.; Vojtek, M.; Vojtekova, J.; Lee, S.; Khoi, D.N.; Nhi, P.T.T.; Dung, T.D. Novel hybrid models between bivariate statistics, artificial neural networks and boosting algorithms for flood susceptibility assessment. *J. Environ. Manag.* **2020**, *265*, 110485. [[CrossRef](#)]
- Nachappa, T.G.; Piralilou, S.T.; Gholamnia, K.; Ghorbanzadeh, O.; Rahmati, O.; Blaschke, T. Flood susceptibility mapping with machine learning, multi-criteria decision analysis and ensemble using Dempster Shafer Theory. *J. Hydrol.* **2020**, *590*, 125275. [[CrossRef](#)]
- Myronidis, D.; Stathis, D.; Sapountzis, M. Post-Evaluation of Flood Hazards Induced by Former Artificial Interventions along a Coastal Mediterranean Settlement. *J. Hydrol. Eng.* **2016**, *21*, 05016022. [[CrossRef](#)]
- Choubin, B.; Moradi, E.; Golshan, M.; Adamowski, J.; Sajedi-Hosseini, F.; Mosavi, A. An ensemble prediction of flood susceptibility using multivariate discriminant analysis, classification and regression trees, and support vector machines. *Sci. Total Environ.* **2019**, *651*, 2087–2096. [[CrossRef](#)]
- Li, F.W.; Wang, L.P.; Zhao, Y. Evolvement rules of basin flood risk under low-carbon mode. Part II: Risk assessment of flood disaster under different land use patterns in the Haihe basin. *Environ. Monit. Assess.* **2017**, *189*, 397. [[CrossRef](#)]
- Liu, J.; Wang, S.Y.; Li, D.M. The Analysis of the Impact of Land-Use Changes on Flood Exposure of Wuhan in Yangtze River Basin, China. *Water Resour. Manag.* **2014**, *28*, 2507–2522. [[CrossRef](#)]
- Lin, W.B.; Sun, Y.M.; Nijhuis, S.; Wang, Z.L. Scenario-based flood risk assessment for urbanizing deltas using future land-use simulation (FLUS): Guangzhou Metropolitan Area as a case study. *Sci. Total Environ.* **2020**, *739*, 139899. [[CrossRef](#)]
- Alfieri, L.; Bisselink, B.; Dottori, F.; Naumann, G.; de Roo, A.; Salamon, P.; Wyser, K.; Feyen, L. Global projections of river flood risk in a warmer world. *Earths Future* **2017**, *5*, 171–182. [[CrossRef](#)]
- Bakker, M.H.N.; Duncan, J.A. Future bottlenecks in international river basins: Where transboundary institutions, population growth and hydrological variability intersect. *Water Int.* **2017**, *42*, 400–424. [[CrossRef](#)]
- Mazzoleni, M.; Bacchi, B.; Barontini, S.; Di Baldassarre, G.; Pilotti, M.; Ranzi, R. Flooding Hazard Mapping in Floodplain Areas Affected by Piping Breaches in the Po River, Italy. *J. Hydrol. Eng.* **2014**, *19*, 717–731. [[CrossRef](#)]

17. Tehrany, M.S.; Jones, S.; Shabani, F. Identifying the essential flood conditioning factors for flood prone area mapping using machine learning techniques. *Catena* **2019**, *175*, 174–192. [[CrossRef](#)]
18. Muis, S.; Guneralp, B.; Jongman, B.; Aerts, J.; Ward, P.J. Flood risk and adaptation strategies under climate change and urban expansion: A probabilistic analysis using global data. *Sci. Total Environ.* **2015**, *538*, 445–457. [[CrossRef](#)]
19. Tehrany, M.S.; Pradhan, B.; Mansor, S.; Ahmad, N. Flood susceptibility assessment using GIS-based support vector machine model with different kernel types. *Catena* **2015**, *125*, 91–101. [[CrossRef](#)]
20. Wang, Z.L.; Lai, C.G.; Chen, X.H.; Yang, B.; Zhao, S.W.; Bai, X.Y. Flood hazard risk assessment model based on random forest. *J. Hydrol.* **2015**, *527*, 1130–1141. [[CrossRef](#)]
21. Kia, M.B.; Pirasteh, S.; Pradhan, B.; Mahmud, A.R.; Sulaiman, W.N.A.; Moradi, A. An artificial neural network model for flood simulation using GIS: Johor River Basin, Malaysia. *Environ. Earth Sci.* **2012**, *67*, 251–264. [[CrossRef](#)]
22. Tehrany, M.S.; Pradhan, B.; Jebur, M.N. Spatial prediction of flood susceptible areas using rule based decision tree (DT) and a novel ensemble bivariate and multivariate statistical models in GIS. *J. Hydrol.* **2013**, *504*, 69–79. [[CrossRef](#)]
23. Tehrany, M.S.; Pradhan, B.; Jebur, M.N. Flood susceptibility mapping using a novel ensemble weights-of-evidence and support vector machine models in GIS. *J. Hydrol.* **2014**, *512*, 332–343. [[CrossRef](#)]
24. Nachappa, T.G.; Meena, S.R. A novel per pixel and object-based ensemble approach for flood susceptibility mapping. *Geomat. Nat. Hazards Risk* **2020**, *11*, 2147–2175. [[CrossRef](#)]
25. Liu, J.F.; Wang, X.Q.; Zhang, B.; Li, J.; Zhang, J.Q.; Liu, X.J. Storm flood risk zoning in the typical regions of Asia using GIS technology. *Nat. Hazards* **2017**, *87*, 1691–1707. [[CrossRef](#)]
26. Zou, Q.; Zhou, J.Z.; Zhou, C.; Song, L.X.; Guo, J. Comprehensive flood risk assessment based on set pair analysis-variable fuzzy sets model and fuzzy AHP. *Stoch. Environ. Res. Risk Assess.* **2013**, *27*, 525–546. [[CrossRef](#)]
27. Lyu, H.M.; Shen, S.L.; Zhou, A.N.; Zhou, W.H. Flood risk assessment of metro systems in a subsiding environment using the interval FAHP-FCA approach. *Sustain. Cities Soc.* **2019**, *50*, 101682. [[CrossRef](#)]
28. Ping, C.; Jian, Z.; Yan, X. Empirical Study on the Influencing Factors of High Technology Industrial Security. *Manag. Rev.* **2017**, *29*, 50–61.
29. Liu, F.; Ma, N. Multicriteria ABC Inventory Classification Using the Social Choice Theory. *Sustainability* **2020**, *12*, 182. [[CrossRef](#)]
30. Jun, K.S.; Chung, E.S.; Kim, Y.G.; Kim, Y. A fuzzy multi-criteria approach to flood risk vulnerability in South Korea by considering climate change impacts. *Expert Syst. Appl.* **2013**, *40*, 1003–1013. [[CrossRef](#)]
31. Song, L.L.; Liu, F. An improvement in DEA cross-efficiency aggregation based on the Shannon entropy. *Int. Trans. Oper. Res.* **2018**, *25*, 705–714. [[CrossRef](#)]
32. An, Y.; Tan, X.C.; Gu, B.H.; Zhu, K.W. Flood risk assessment using the CV-TOPSIS method for the Belt and Road Initiative: An empirical study of Southeast Asia. *Ecosyst. Health Sustain.* **2020**, *6*, 1765703. [[CrossRef](#)]
33. Govindan, K.; Khodaverdi, R.; Jafarian, A. A fuzzy multi criteria approach for measuring sustainability performance of a supplier based on triple bottom line approach. *J. Clean. Prod.* **2013**, *47*, 345–354. [[CrossRef](#)]
34. Yang, W.C.; Xu, K.; Lian, J.J.; Ma, C.; Bin, L.L. Integrated flood vulnerability assessment approach based on TOPSIS and Shannon entropy methods. *Ecol. Indic.* **2018**, *89*, 269–280. [[CrossRef](#)]
35. Zhu, H.G.; Liu, F. A Group-Decision-Making Framework for Evaluating Urban Flood Resilience: A Case Study in Yangtze River. *Sustainability* **2021**, *13*, 665. [[CrossRef](#)]
36. Sun, W.C.; Wang, J.; Li, Z.J.; Yao, X.L.; Yu, J.S. Influences of Climate Change on Water Resources Availability in Jinjiang Basin, China. *Sci. World J.* **2014**, *2014*, 908349. [[CrossRef](#)]
37. Wu, H.F.; Chen, Y.; Chen, X.W.; Liu, M.B.; Gao, L.; Deng, H.J. A New Approach for Optimizing Rain Gauge Networks: A Case Study in the Jinjiang Basin. *Water* **2020**, *12*, 2252. [[CrossRef](#)]
38. Yang, T.H.; Yang, S.C.; Ho, J.Y.; Lin, G.F.; Hwang, G.D.; Lee, C.S. Flash flood warnings using the ensemble precipitation forecasting technique: A case study on forecasting floods in Taiwan caused by typhoons. *J. Hydrol.* **2015**, *520*, 367–378. [[CrossRef](#)]
39. Huang, D.; Zhang, L. Assessment of Rainstorm Disaster-causing Force of Flood Risk in Central and Eastern China. In Proceedings of the 7th Annual Meeting of Risk Analysis Council of China Association for Disaster Prevention (RAC-2016), Changsha, China, 4–6 November 2016; pp. 200–205.
40. Mohamoud, Y.M. Evaluating Manning’s roughness coefficients for tilled soils. *J. Hydrol.* **1992**, *135*, 143–156. [[CrossRef](#)]
41. Vojtek, M.; Vojtekova, J. Flood Susceptibility Mapping on a National Scale in Slovakia Using the Analytical Hierarchy Process. *Water* **2019**, *11*, 17. [[CrossRef](#)]
42. Costache, R.; Dieu Tien, B. Identification of areas prone to flash-flood phenomena using multiple-criteria decision-making, bivariate statistics, machine learning and their ensembles. *Sci. Total Environ.* **2020**, *712*, 136492. [[CrossRef](#)]
43. Chapi, K.; Singh, V.P.; Shirzadi, A.; Shahabi, H.; Bui, D.T.; Pham, B.T.; Khosravi, K. A novel hybrid artificial intelligence approach for flood susceptibility assessment. *Environ. Model. Softw.* **2017**, *95*, 229–245. [[CrossRef](#)]
44. Arora, A.; Arabameri, A.; Pandey, M.; Siddiqui, M.A.; Shukla, U.K.; Bui, D.T.; Mishra, V.N.; Bhardwaj, A. Optimization of state-of-the-art fuzzy-metaheuristic ANFIS-based machine learning models for flood susceptibility prediction mapping in the Middle Ganga Plain, India. *Sci. Total Environ.* **2021**, *750*, 141565. [[CrossRef](#)]
45. Del Giudice, G.; Padulano, R.; Rasulo, G. Spatial prediction of the runoff coefficient in Southern Peninsular Italy for the index flood estimation. *Hydrol. Res.* **2014**, *45*, 263–281. [[CrossRef](#)]
46. Sriwongsitanon, N.; Taesombat, W. Effects of land cover on runoff coefficient. *J. Hydrol.* **2011**, *410*, 226–238. [[CrossRef](#)]

47. Hu, S.S.; Cheng, X.J.; Zhou, D.M.; Zhang, H. GIS-based flood risk assessment in suburban areas: A case study of the Fangshan District, Beijing. *Nat. Hazards* **2017**, *87*, 1525–1543. [[CrossRef](#)]
48. Dandapat, K.; Panda, G.K. Flood vulnerability analysis and risk assessment using analytical hierarchy process. *Modeling Earth Syst. Environ.* **2017**, *3*, 1627–1646. [[CrossRef](#)]
49. Li, X.; Lin, S. Analysis of the Relationship between Local Fiscal Revenue and Economic Growth—Wuhan City, Hubei Province as an Example. *Caizhengjiandu* **2020**, *464*, 80–90.
50. Arsanjani, J.J.; Helbich, M.; Kainz, W.; Bolorani, A.D. Integration of logistic regression, Markov chain and cellular automata models to simulate urban expansion. *Int. J. Appl. Earth Obs. Geoinf.* **2013**, *21*, 265–275. [[CrossRef](#)]
51. Lu, R.; Huang, X.; Zhuo, T.; Xiao, S.; Zhao, X.; Zhang, X. Land Use Scenarios Simulation Based on CLUE-S and Markov Composite Model—A Case Study of Taihu Lake Rim in Jiangsu Province. *Sci. Geogr. Sin.* **2009**, *29*, 577–581.
52. Hu, S.; Chen, L.Q.; Li, L.; Zhang, T.; Yuan, L.N.; Cheng, L.; Wang, J.; Wen, M.X. Simulation of Land Use Change and Ecosystem Service Value Dynamics under Ecological Constraints in Anhui Province, China. *Int. J. Environ. Res. Public Health* **2020**, *17*, 4228. [[CrossRef](#)]
53. Liu, X.P.; Liang, X.; Li, X.; Xu, X.C.; Ou, J.P.; Chen, Y.M.; Li, S.Y.; Wang, S.J.; Pei, F.S. A future land use simulation model (FLUS) for simulating multiple land use scenarios by coupling human and natural effects. *Landsc. Urban. Plan.* **2017**, *168*, 94–116. [[CrossRef](#)]
54. Dong, N.; You, L.; Cai, W.J.; Li, G.; Lin, H. Land use projections in China under global socioeconomic and emission scenarios: Utilizing a scenario-based land-use change assessment framework. *Glob. Environ. Chang. Hum. Policy Dimens.* **2018**, *50*, 164–177. [[CrossRef](#)]
55. Liao, W.L.; Liu, X.P.; Xu, X.Y.; Chen, G.Z.; Liang, X.; Zhang, H.H.; Li, X. Projections of land use changes under the plant functional type classification in different SSP-RCP scenarios in China. *Sci. Bull.* **2020**, *65*, 1935–1947. [[CrossRef](#)]
56. Chen, Z.Z.; Huang, M.; Zhu, D.Y.; Altan, O. Integrating Remote Sensing and a Markov-FLUS Model to Simulate Future Land Use Changes in Hokkaido, Japan. *Remote Sens.* **2021**, *13*, 2621. [[CrossRef](#)]
57. Liang, X.; Liu, X.P.; Li, X.; Chen, Y.M.; Tian, H.; Yao, Y. Delineating multi-scenario urban growth boundaries with a CA-based FLUS model and morphological method. *Landsc. Urban. Plan.* **2018**, *177*, 47–63. [[CrossRef](#)]
58. Lai, Y.; Huang, G.Q.; Chen, S.Z.; Lin, S.T.; Lin, W.J.; Lyu, J.X. Land Use Dynamics and Optimization from 2000 to 2020 in East Guangdong Province, China. *Sustainability* **2021**, *13*, 3473. [[CrossRef](#)]
59. Kundu, S.; Mondal, A.; Khare, D.; Hain, C.; Lakshmi, V. Projecting Climate and Land Use Change Impacts on Actual Evapotranspiration for the Narmada River Basin in Central India in the Future. *Remote Sens.* **2018**, *10*, 578. [[CrossRef](#)]
60. Myronidis, D.; Ioannou, K. Forecasting the Urban Expansion Effects on the Design Storm Hydrograph and Sediment Yield Using Artificial Neural Networks. *Water* **2019**, *11*, 31. [[CrossRef](#)]
61. Gounaridis, D.; Chorianopoulos, I.; Symeonakis, E.; Koukoulas, S. A Random Forest-Cellular Automata modelling approach to explore future land use/cover change in Attica (Greece), under different socio-economic realities and scales. *Sci. Total Environ.* **2019**, *646*, 320–335. [[CrossRef](#)]
62. Wang, L. Change and Simulation of Land Use in Longnan City Based on FLUS Model. Master's Thesis, Northwest Normal University, Lanzhou, China, 2020.
63. Li, J.Y.; Gong, J.; Guldman, J.M.; Li, S.C.; Zhu, J. Carbon Dynamics in the Northeastern Qinghai-Tibetan Plateau from 1990 to 2030 Using Landsat Land Use/Cover Change Data. *Remote Sens.* **2020**, *12*, 528. [[CrossRef](#)]
64. Wang, L.T.; Wang, S.X.; Zhou, Y.; Liu, W.L.; Hou, Y.F.; Zhu, J.F.; Wang, F.T. Mapping population density in China between 1990 and 2010 using remote sensing. *Remote Sens. Environ.* **2018**, *210*, 269–281. [[CrossRef](#)]
65. Zeng, C.Q.; Zhou, Y.; Wang, S.X.; Yan, F.L.; Zhao, Q. Population spatialization in China based on night-time imagery and land use data. *Int. J. Remote Sens.* **2011**, *32*, 9599–9620. [[CrossRef](#)]
66. Liao, S.; Sun, J. GIS Based Spatialization of Population Census Data in Qinghai—Tibet Plateau. *Acta Geogr. Sin.* **2003**, *58*, 25–33. [[CrossRef](#)]
67. Zheng, Q.; Lyu, H.M.; Zhou, A.N.; Shen, S.L. Risk assessment of geohazards along Cheng-Kun railway using fuzzy AHP incorporated into GIS. *Geomat. Nat. Hazards Risk* **2021**, *12*, 1508–1531. [[CrossRef](#)]
68. Liu, H.M.; Zhou, W.H.; Shen, S.L.; Zhou, A.N. Inundation risk assessment of metro system using AHP and TFN-AHP in Shenzhen. *Sustain. Cities Soc.* **2020**, *56*, 102103. [[CrossRef](#)]
69. Shi, L.Q.; Qiu, M.; Teng, C.; Wang, Y.; Liu, T.H.; Qu, X.Y. Risk assessment of water inrush to coal seams from underlying aquifer by an innovative combination of the TFN-AHP and TOPSIS techniques. *Arab. J. Geosci.* **2020**, *13*, 600. [[CrossRef](#)]
70. Deng, H. Multicriteria analysis with fuzzy pairwise comparison. *Int. J. Approx. Reason.* **1999**, *21*, 215–231. [[CrossRef](#)]
71. Diakoulaki, D.; Mavrotas, G.; Papayannakis, L. Determining objective weights in multiple criteria problems: The critic method. *Comput. Oper. Res.* **1995**, *22*, 763–770. [[CrossRef](#)]
72. Ding, X.; Zhang, D. K-Means Algorithm Based on Synthetic Weighting of AHP and CRITIC. *Comput. Syst. Appl.* **2016**, *25*, 182–186. [[CrossRef](#)]
73. Hwang, C.L.; Yoon, K. *Multiple Attribute Decision Making: Methods and Applications*; Springer: Berlin/Heidelberg, Germany, 1981.
74. Mao, N.; Song, M.J.; Deng, S.M. Application of TOPSIS method in evaluating the effects of supply vane angle of a task/ambient air conditioning system on energy utilization and thermal comfort. *Appl. Energy* **2016**, *180*, 536–545. [[CrossRef](#)]
75. Liu, W.; Zhan, J.Y.; Zhao, F.; Yan, H.M.; Zhang, F.; Wei, X.Q. Impacts of urbanization-induced land-use changes on ecosystem services: A case study of the Pearl River Delta Metropolitan Region, China. *Ecol. Indic.* **2019**, *98*, 228–238. [[CrossRef](#)]

76. Waghwala, R.K.; Agnihotri, P.G. Flood risk assessment and resilience strategies for flood risk management: A case study of Surat City. *Int. J. Disaster Risk Reduct.* **2019**, *40*, 101155. [[CrossRef](#)]
77. Wan, L.; Ye, X.; Lee, J.; Lu, X.; Zheng, L. Effects of urbanization on ecosystem service values in a mineral resource-based city. *Habitat Int.* **2015**, *46*, 54–63. [[CrossRef](#)]
78. Hu, S.; Chen, L.Q.; Li, L.; Wang, B.Y.; Yuan, L.N.; Cheng, L.; Yu, Z.Q.; Zhang, T. Spatiotemporal Dynamics of Ecosystem Service Value Determined by Land-Use Changes in the Urbanization of Anhui Province, China. *Int. J. Environ. Res. Public Health* **2019**, *16*, 5104. [[CrossRef](#)]
79. Zhang, X.; Li, A.; Nan, X.; Lei, G.; Wang, C. Multi-scenario Simulation of Land Use Change Along China-Pakistan Economic Corridor through Coupling FLUS Model with SD Model. *J. Geo-Inf. Sci.* **2020**, *22*, 17.
80. Villarreal-Rosas, J.; Wells, J.A.; Sonter, L.J.; Possingham, H.P.; Rhodes, J.R. The impacts of land use change on flood protection services among multiple beneficiaries. *Sci. Total Environ.* **2022**, *806*, 150577. [[CrossRef](#)]
81. Rounsevell, M.D.A.; Metzger, M.J. Developing qualitative scenario storylines for environmental change assessment. *Wiley Interdiscip. Rev. Clim. Chang.* **2010**, *1*, 606–619. [[CrossRef](#)]
82. Szwagrzyk, M.; Kaim, D.; Price, B.; Wypych, A.; Grabska, E.; Kozak, J. Impact of forecasted land use changes on flood risk in the Polish Carpathians. *Nat. Hazards* **2018**, *94*, 227–240. [[CrossRef](#)]
83. Greeuw, S.; Asselt, M.V.; Grosskurth, J. *Cloudy Crystal Balls: An Assessment of Recent European and Global Scenario Studies and Models*; European Environment Agency: Copenhagen, Denmark, 2000.
84. Murray-Rust, D.; Rieser, V.; Robinson, D.T.; Milicic, V.; Rounsevell, M. Agent-based modelling of land use dynamics and residential quality of life for future scenarios. *Environ. Model. Softw.* **2013**, *46*, 75–89. [[CrossRef](#)]
85. Thieken, A.H.; Cammerer, H.; Dobler, C.; Lammel, J.; Schoberl, F. Estimating changes in flood risks and benefits of non-structural adaptation strategies—A case study from Tyrol, Austria. *Mitig. Adapt. Strateg. Glob. Chang.* **2016**, *21*, 343–376. [[CrossRef](#)]
86. Tellman, B.; Saiers, J.E.; Cruz, O.A.R. Quantifying the impacts of land use change on flooding in data-poor watersheds in El Salvador with community-based model calibration. *Reg. Environ. Chang.* **2016**, *16*, 1183–1196. [[CrossRef](#)]
87. Huong, H.T.L.; Pathirana, A. Urbanization and climate change impacts on future urban flooding in Can Tho city, Vietnam. *Hydrol. Earth Syst. Sci.* **2013**, *17*, 379–394. [[CrossRef](#)]
88. Rapalo, L.M.C.; Uliana, E.M.; Moreira, M.C.; da Silva, D.D.; Ribeiro, C.B.D.; da Cruz, I.F.; Pereira, D.D. Effects of land-use and -cover changes on streamflow regime in the Brazilian Savannah. *J. Hydrol. Reg. Stud.* **2021**, *38*, 100934. [[CrossRef](#)]